PROJECTIONS OF POTENTIAL FLOOD REGIME CHANGES IN CALIFORNIA

A Report From:
California Climate Change Center

Prepared By:
Michael Dettinger[1,2], Hugo Hidalgo[2], Tapash Das[2], Daniel Cayan[1,2], and Noah Knowles[3]

[1] U.S. Geological Survey, La Jolla, California
[2] Scripps Institution of Oceanography
[3] U.S. Geological Survey, Menlo Park, California

FINAL PAPER

DISCLAIMER

This paper was prepared as the result of work sponsored by the California Energy Commission (Energy Commission) and the California Environmental Protection Agency (Cal/EPA). It does not necessarily represent the views of the Energy Commission, Cal/EPA, their employees, or the State of California. The Energy Commission, Cal/EPA, the State of California, their employees, contractors, and subcontractors make no warrant, express or implied, and assume no legal liability for the information in this paper; nor does any party represent that the uses of this information will not infringe upon privately owned rights. This paper has not been approved or disapproved by the California Energy Commission or Cal/EPA, nor has the California Energy Commission or Cal/EPA passed upon the accuracy or adequacy of the information in this paper.

Arnold Schwarzenegger, *Governor*

August 2009
CEC-500-2009-050-F

Acknowledgments

Research described in Section 5 was supported by both the California Energy Commission-funded California Climate Change Center and the CALFED Bay-Delta Program-funded Computational Assessments of Scenarios of Change in the Delta Ecosystem (CASCaDE) Project.

"This was the most sublime waterfall flood I ever saw—clouds, winds, rocks, waters, throbbing together as one. And then to contemplate what was going on simultaneously with all this in other mountain temples; the Big Tuolumne Canyon—how the white waters and the winds were singing there! And in Hetch Hetchy Valley and the great King's River yosemite, and in all the other Sierra canyons and valleys from Shasta to the southernmost fountains of the Kern, thousands of rejoicing flood waterfalls chanting together in jubilee dress." — John Muir describing the December 18, 1871, flood in Yosemite Valley, in The Yosemite, *1914, pp. 39–44.*

Preface

The California Energy Commission's Public Interest Energy Research (PIER) Program supports public interest energy research and development that will help improve the quality of life in California by bringing environmentally safe, affordable, and reliable energy services and products to the marketplace.

The PIER Program conducts public interest research, development, and demonstration (RD&D) projects to benefit California's electricity and natural gas ratepayers. The PIER Program strives to conduct the most promising public interest energy research by partnering with RD&D entities, including individuals, businesses, utilities, and public or private research institutions.

PIER funding efforts focus on the following RD&D program areas:

- Buildings End-Use Energy Efficiency
- Energy-Related Environmental Research
- Energy Systems Integration
- Environmentally Preferred Advanced Generation
- Industrial/Agricultural/Water End-Use Energy Efficiency
- Renewable Energy Technologies
- Transportation

In 2003, the California Energy Commission's PIER Program established the **California Climate Change Center** to document climate change research relevant to the states. This center is a virtual organization with core research activities at Scripps Institution of Oceanography and the University of California, Berkeley, complemented by efforts at other research institutions. Priority research areas defined in PIER's five-year Climate Change Research Plan are: monitoring, analysis, and modeling of climate; analysis of options to reduce greenhouse gas emissions; assessment of physical impacts and of adaptation strategies; and analysis of the economic consequences of both climate change impacts and the efforts designed to reduce emissions.

The California Climate Change Center Report Series details ongoing center-sponsored research. As interim project results, the information contained in these reports may change; authors should be contacted for the most recent project results. By providing ready access to this timely research, the center seeks to inform the public and expand dissemination of climate change information, thereby leveraging collaborative efforts and increasing the benefits of this research to California's citizens, environment, and economy.

For more information on the PIER Program, please visit the Energy Commission's website www.energy.ca.gov/pier/ or contract the Energy Commission at (916) 654-5164.

Table of Contents

Preface.. iii
Abstract xi
1.0 Introduction 1
2.0 Flood Mechanisms and Warming in the Sierra Nevada 3
2.1. Historical Floods 3
2.2. Rainfall-Runoff Contributing Areas 8
2.3. Rain on Snow 11
2.4. Antecedent Soil Moisture 13
2.5. Synchronous Springtime Snowmelt 14
3.0 Projections of Future Atmospheric-River Storms 14
4.0 Hydrologic Simulation Analysis of Sierra Nevadan Floods 29
4.1. Method 29
4.2. Simulations of Changing Flood Risks 31
4.2.1. Northern Sierra Nevada 31
4.2.2. Southern Sierra Nevada 38
4.3. Summary 41
5.0 Tides, Storm Surges, and Floods 42
6.0 Conclusions 46
7.0 References 48
8.0 Glossary 53

List of Figures

Figure 1. (a) Daily discharges of the Merced River at Happy Isles, Yosemite Valley, 1916–2005, with seasonality of major floods indicated; (b) daily temperatures and precipitation totals in Yosemite Valley during Decembers and Januaries, 1915–1999, with solid dots indicating large floods from panel (a) and open circles and single asterisk indicating storms of similar magnitude that did not yield floods 4

Figure 2. Water-year-to-date precipitation totals and flood discharges in Yosemite Valley associated with selected (symboled) days in Figure 1b; dashed ovals indicate general distribution of discharge episodes with dry antecedent (red) and wet (blue) soils 5

Figure 3. Daily precipitation totals at three precipitation gages in Yosemite National Park, from California Department of Water Resources California Data Exchange Center (left panel) and temperatures at the end (coldest part) of the May 16, 2005, storm from Scripps/USGS Hydroclimatic Monitoring Network in the park, along with long-term average winter-storm temperatures (based on temperatures at Yosemite Valley and assumed -6.5ºC (20.3ºF)/kilometer (km) temperature lapse rates) and temperatures during New Years 1997 storm (extrapolated from temperatures measured in Yosemite Valley and at Twin Lake, 2440 m elevation) (right panel) 6

Figure 4. Snow-water contents measured by snow pillows at three locations in Yosemite National Park during May 2005; data from California Department of Water Resources California Data Exchange Center 7

Figure 5. Map of Yosemite National Park, showing areas that typically receive rain in winter storms (green), that received rain on May 16, 2005 (blue), and that received snow on May 16, 2005 (dark blue); the topography of Yosemite National Park is such that its western edge is at a lower altitude (about 1200 m) than its eastern boundary at the Sierra Nevada ridgeline (about 3000 m to 3700 m) 8

Figure 6. Altitude-area distributions (hypsographs) of four Sierra Nevada river basins. The blue shaded band is roughly the zone within which rain is sometimes deposited under the current climate, but snow is more common. 9

Figure 7. Fractions of historical (black curves) and warmer (red curves) wet days on which rain might be deposited on various fractions of the Merced River basin (above Yosemite Valley, top panel) and of the North Fork American River basin (above North Fork Dam, bottom panel). The warmer scenarios are simply the historical record from each, augmented by a uniform +3ºC (+5.4ºF) warming. The method used to estimate these fractions is described in text. 11

Figure 8. Simulated differences in soil-moisture contents in the upper 5 cm of soil column between a simulation of hydrologic variability driven by historical meteorology, Decembers and Januaries 1950–1999, and a similar simulation but with temperatures uniformly elevated by +2ºC (+3.6ºF); simulations were made with the Variable Infiltration Capacity (VIC) land-surface hydrology model on a 12-km grid. Notice that color bar

representing reduction in soil moisture with warming (reds) is expanded by a factor of ten relative to the color bar for soil-moisture increases (blues). 13

Figure 9. (Top) Special Sensor Microwave/Imager (SSM/I) integrated water vapor imagery from GMT morning on 2 January 1997. (Middle left) Infrared weather-satellite imagery of the Pacific Ocean basin (GOES-West) from 1800 hours GMT on 1 January 1997, and (middle right) a corresponding daily weather map. (Bottom) Vertically integrated water-vapor transport directions and relative rates. The arrow at the bottom indicates the length of a 1000 kg/m/s transport. 16

Figure 10. (a) Plot of daily December–February integrated water vapor (IWV) and upslope wind values from GFDL CM2.1 climate model, and (b) numbers of days per winter falling into the upper right quadrant of that plot, under evolving 20th- and 21st-century climate changes with A2 greenhouse gas emissions 19

Figure 11. Numbers of December–February days per year in the upper-right quadrant of Figure 10a, for seven climate models and the NCAR-NCEP Reanalysis data fields; 21st century counts are from projections made in response to A2 emissions scenarios 19

Figure 12. Histograms of simulated historical (20c3m, black) and future (A2, green and red) distributions of integrated water vapor values associated with AR-days in seven climate models 22

Figure 13. Same as Figure 12, except for upslope winds on AR days 23

Figure 14. Same as Figure 12, except for intensities (IWV * upslope wind) on AR days 24

Figure 15. Ensemble average temperatures on December–February AR days (red) and on all December–February days (blue) under conditions corresponding to Figures 12–14 26

Figure 16. Same as Figure 12, except for surface-air temperatures on AR days 27

Figure 17. Simulated historical and projected (under A2 emissions) numbers of AR-days for each day of the calendar year; panels and coloring as in Figure 12. All curves have been smoothed with a 14-day moving average. 28

Figure 18. Ensembles of historical and future temperature and precipitation projections from three coupled ocean-atmosphere general circulation models, each forced by historical and 21st century A2 greenhouse gas emission scenarios; solid curves are seven-year moving averages, and dashed curves are annual deviations 30

Figure 19. Floods in California's northern Sierra Nevada (a) and southern Sierra Nevada (b). In the figures, "X" symbols are precipitation-driven floods and red circle are snowmelt driven floods. Basin areas contributing to the floods are shown in inset maps. 32

Figure 20. Composites of the 10 most extreme streamflow events occurring in Decembers–Februaries in the northern Sierra Nevada: (a) 700 mbar geopotential height anomalies (Z700); (b) 700 mbar mean wind speeds (U700); and (c) precipitable water (PW). In the panels, day 0 indicates the day of the flood events and day -3 indicated three days before the events. The panels were created using online compositing tools provided by NOAA's Climate Diagnostics Center. 33

Figure 21. Frequency of the three-day annual maximum streamflows for the 1950–1999 period in the northern Sierra Nevada (a) and southern Sierra Nevada (b) 34

Figure 22. Frequency of the three-day annual maximum streamflows in the northern Sierra Nevada under climate change projections from three coupled ocean-atmosphere general circulation models, each forced by historical (blue curves) and 21st century greenhouse-gas A2 emission scenarios (red).....35

Figure 23. Same as Figure 22, except for the southern Sierra Nevada 36

Figure 24. Floods in northern Sierra Nevada (a) and southern Sierra Nevada (b) in the 21st century, as simulated by the CNRM CM3 global climate models under 21st century A2 emissions scenario; "X" symbols are precipitation-driven floods and red circles are snowmelt driven floods 39

Figure 25. Same as Figure 24, except for simulation by the GFDL CM2.1 global climate model .40

Figure 26. Same as Figure 24, except for simulation by the NCAR PCM global climate model..41

Figure 27. Simulated reservoir inflows in the Sacramento and San Joaquin River basins, from the Bay-Delta Watershed Model (Knowles and Cayan 2002) driven by simulated historical (20c3m) and future (A2 greenhouse-gas emissions) climates from the GFDL global climate model, downscaled by the constructed analogues method (Hidalgo et al. 2008).....44

Figure 28. Simulated freshwater reservoir inflows in the Sacramento and San Joaquin River basins during days when projected sea levels are at or above the 1950–2005 99.9% exceedance level at San Francisco, under climatic conditions projected by the GFDL CM2.1 global climate model under historical and A2 greenhouse-gas emissions scenarios. Streamflows shown here are from the simulation displayed in Figure 27. 45

List of Tables

Table 1. Counts of December–February days with IWV > 2.5 cm and upslope winds > 10 m/s in an ensemble of projections of climate change under an historical and A2-future emissions scenario from seven GCMs and in the NCAR-NCEP historical Reanalysis dataset; GCMs are the CCC CGCM3.1 (Canadian), CNRM CM3 (French), ECHAM 5 (German), GFDL CM2.1 (US), GISS Er (US), MIROC medium-resolution (Japanese), and MRI CGCM2.3 (Japanese) climate models 20

Table 2. Trends in numbers of AR days / 100 years from seven climate models, with trends that rise to statistical significance at 95% level highlighted in boldface, and with (*) the trend in the CNRM model only just missing the 95% significance level.....20

Table 3. Trends in intensity (IWV * upslope wind speed) of AR days / 100 years from seven climate models, with trends that rise to statistical significance at 95% level highlighted in boldface, and with (*) the trend in MRI only just missing 95% significance level.....21

Table 4. Three-day maximum floods from flood frequency analyses using log-Pearson III distributions; boldface where statistically different from floods in 1950–1999 period 37

Abstract

Floods have been a recurring theme in California's climatology, hydrology, and politics throughout its history. Today, California's aging water supply and flood protection infrastructures are challenged by major floods and increased standards for urban flood protection. With warming in the twenty-first century, some changes in California's flood regimes seem likely: Higher snowlines may well increase the frequency of flooding; occasional larger than historical flood magnitudes are likely to follow—especially from the higher southern parts of the Sierra Nevada; potentials for floods may be exacerbated by wetter winter soils in high-altitude catchments; and opportunities for estuarine and coastal flooding may increase as sea-level rise and flood frequencies converge. Other changes are more difficult to project, and simulation models are used here to weigh competing influences that might either increase or diminish future floods. Both the Variable Infiltration Capacity (VIC) and Bay-Delta Watershed Model (BDWM) hydrologic models responded to downscaled climate-change projections with increases in flood frequencies and magnitudes, but neither yielded large changes in that regard, especially in the northern parts of the state. Future characteristics of major storms, in particular pineapple express or atmospheric river storms, by global climate models indicated changes mostly at the extremes: Years with many atmospheric river storms become more frequent in most climate models analyzed here, but the average number of such storms per year did not change much. Likewise, although the average intensity of storms was not projected to increase much in most climate models, occasional much-larger-than-historical-range storm intensities were simulated.

Keywords: California, floods, climate change, hydrologic change, simulations, atmospheric rivers, sea-level rise

1.0 Introduction

Major floods are a recurring theme in California's climatology and hydrology, and they have a long history of being an important cause of death and destruction in California (Kelley 1998). Even today, California's aging water supply and flood protection infrastructure, including more than a thousand kilometers of levees, is being challenged by punishing floods and increased standards for urban flood protection. Many Californians face unacceptable risks from flooding, both from where they live and work and from where they derive water supplies. In the Delta of the Sacramento and San Joaquin Rivers and in nearby communities, including the city of Sacramento, a major flood could even unleash the Californian equivalent of 2005's Hurricane Katrina, inundating communities and disrupting critical water infrastructure for the entire state.[1] In addition, a seemingly inevitable conflict exists between providing flood protection and the other functions of major water storage facilities in California: water supply, water quality, hydropower generation, water temperature and flow for at risk species, and recreation. Flood protection is provided by keeping empty flood control storage space behind the dams during the flood season. The other users require fuller reservoirs, if possible. Thus, moves to provide more water supplies, or more reliable water supplies, frequently are at odds with the requirements of flood control.

In response to the acknowledged risks and conflicts posed by flooding, the California Department of Water Resources Water Plan Updates in both 2005 and 2009 strongly recommend that water supply management, land use development, and flood management in the state be much more fully integrated (DWR 2005, 2009). The Delta Vision Blue Ribbon Task Force has identified improvements in floodplain and flood emergency management among its key recommendations for the future of California's Delta (Delta Vision Task Force 2008). Perhaps most convincingly, the people of California passed Propositions 1E and 84 in 2006 to fund bonds intended to provide over $4.5 billion dollars specifically for flood management programs in the state. Much current interest emphasizes the Delta and Central Valley, where flood disasters threaten urban, suburban, and rural communities and infrastructure, and threaten critical north-to-south (and east-to-west) linkages in major state, federal, and local water-supply systems. Population growth and urbanization in the Delta and Central Valley are only increasing the risks from floods in the regions. Other parts of the state are similarly, if generally more locally, at risk from extreme floods, so that programs to address flood management in the state (such as the FloodSAFE Program)[2] are frequently statewide in their scopes.

Although uncertainties abound, the challenges of flood control in California may become more commonplace or extreme as a result of projected climate changes due to increasing greenhouse-gas concentrations in the global atmosphere. Current climate change projections for twenty-first century California uniformly include warming by at least a couple of degrees, and, although great uncertainties exist about future changes in long-term average precipitation rates in California (e.g., Dettinger 2005; Cayan et al. 2008a) it is generally expected that extreme precipitation episodes may become more extreme as the climate changes (Cayan et al. 2008b).

---

[1] www.terradaily.com/reports/Scientists_Say_California_Quake_Could_Cause_Katrina_II.html

[2] www.water.ca.gov/floodsafe/docs/FloodSAFE_Overview_Fact_Sheet.pdf

These changes in extremes, together with other changes in atmospheric circulation patterns and other variables, may well change California's flood regimes in a number of ways, such as:

- Potential for intensification or amelioration of floods (bigger floods or smaller floods?)
- Potential for increased, or decreased, frequencies of floods (more floods or less floods?)
- Potential for changing seasonalities and mechanisms of floods?

In each case, which way these changes will trend remains quite uncertain. For example, arguments can be made that, with more water vapor and heat in the atmosphere, storms and thus floods will become more intense (e.g., Trenberth 1999) or larger overall; however, as the polar regions warm more quickly than the lower latitudes, the equator-to-pole temperature differences are expected to decrease (Jain et al. 1999) which generally would be expected—from basic geophysical fluid dynamics considerations—to weaken midlatitude storm tracks.

Which change will dominate California's future flood regimes? Because the humid tropics have the strongest greenhouse effect, more heat will need to be transported poleward as the world warms so that midlatitude storms (which are an important mechanism for poleward heat transports) may become more frequent. Alternatively, though, as noted previously, declining equator-to-pole temperature differences might also tend to weaken storm tracks and reduce storm frequencies. Even in such a scenario of weakening storm tracks, however, trends toward warmer storms may change much precipitation from snow to rain (Knowles et al. 2006), changing the mechanisms and opportunities for flood generation in California's higher and wetter catchments in ways that increase the percentage of storms that generate floods. In such a case, would weakening storm tracks or increasing rain fractions dominate to decrease or increase the numbers of overall floods? In a warming region, with presumed increases in the demands and opportunities for evaporation and transpiration, soils are likely to generally be drier (unless total precipitation increases considerably), which could reduce risks of floods. Alternatively, though, as long as there is *some* snow still being deposited in the state, it is likely that warmer winters—at least—may induce more mid-winter snowmelt and thus wetter soils in winter, which might make flooding more likely.

Given these many tensions between conditions that might reduce flooding and conditions that might increase flooding as California's climate changes in response to increasing global greenhouse-gas concentrations, it is difficult to confidently decide, or even intuit, the eventual outcome with respect to future flood regimes. Confronted with such competing influences and little historical signal to provide guidance, process-based models—both of climatic and hydrologic processes—are perhaps the most useful, immediate step toward predicting future flood regimes. Analysis of model simulations of storms and floods under future climates is unlikely to be the final step in understanding or predicting future flood regimes, because after all they are just models. Analyses of simulated future flood regimes will, we hope, provide useful guidance, hypotheses, and directions for future research that will bolster our confidence in both our models and understanding of California's future floods. In this paper, some basic ways that warming alone (without specific changes in precipitation) might be expected to change flood conditions will be reviewed in Section 2. In Section 3, the future of a specific subset of flood-generating storms—the pineapple expresses or atmospheric-river storms—will be characterized using projections from seven current climate models. Climate-change projections from three climate models will be downscaled and used to force the Variable Infiltration

Capacity hydrologic model in Section 4, wherein potential changes in flood frequencies and mechanisms will be reported. In Section 5, projected changes in the frequency of concurrent high sea-level stands with high flood flows in the Sacramento-San Joaquin Delta will be investigated for a particularly warm and challenging climate projection. Finally some overall observations about the likely future of California's regimes will be discussed in Section 6.

2.0 Flood Mechanisms and Warming in the Sierra Nevada

Climate change may change California's flood magnitudes and frequencies, and even the mechanisms by which floods are unleashed, in a variety of ways. Tendencies toward larger storm precipitation totals or more frequent large storms, or the reverse, could directly change the opportunities for floods. Projected warming trends may result in continuations of recent trends toward having more precipitation fall as rain and less as snow (Knowles et al. 2006), which could effect both magnitudes and frequencies of flood, especially from the highest catchments in the state, by increasing the catchment areas from which precipitation (rain) runs off most rapidly or by increasing the frequency of storms in which rainfall runoff totals are large. Warming may also change catchment water balances in ways that might alter antecedent hydrologic conditions that set the stage for floods, e.g., by increasing rates and opportunities for evapotranspiration to sap soil-moisture reservoirs. In this section, some of the more direct potential effects of warming on flooding from the Sierra Nevada catchments will be discussed, as a conceptual background for subsequent discussions of simulation analyses.

2.1. Historical Floods

In much of Central and Northern California, especially in the Sierra Nevada, the largest recorded flood at most stream gages occurred just after New Years 1997 (e.g., Figure 1a). The storm that resulted in these record-breaking floods was at the end of a string of storms that had saturated many soils and land surfaces, and that had laid down snowfields to unusually low altitudes. The New Year storm, however, was very warm (for that time of year, Figure 1b) and much of its destructive power arose from the fact that rain fell to very high altitudes; e.g., the snowline was estimated from middle altitude stations in the central Sierra and concurrent temperature lapse rates to be at or above 3000 meters (m) above sea level. The New Year storm also dropped large amounts of precipitation (e.g., Figure 1b).

(a)

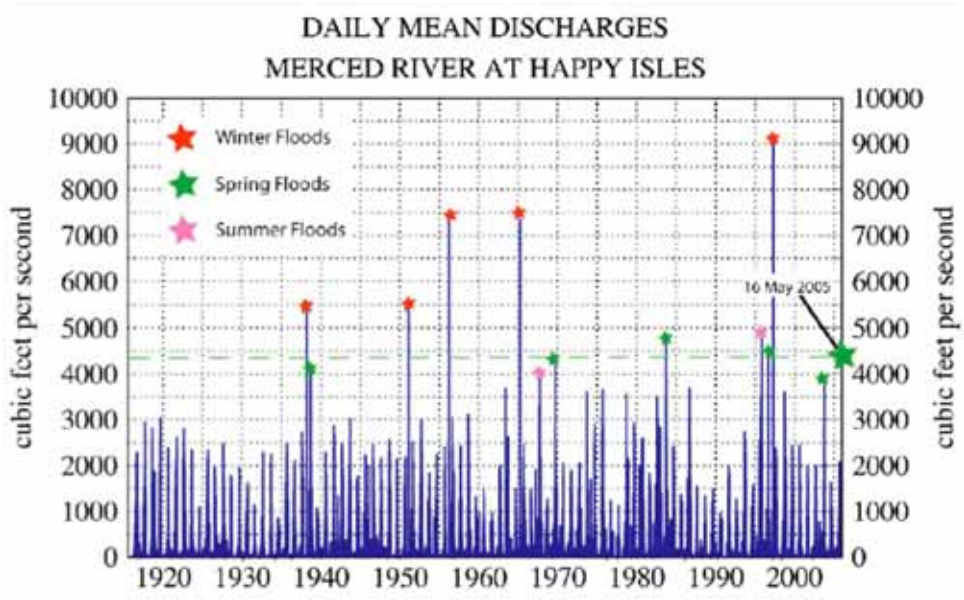

(b)

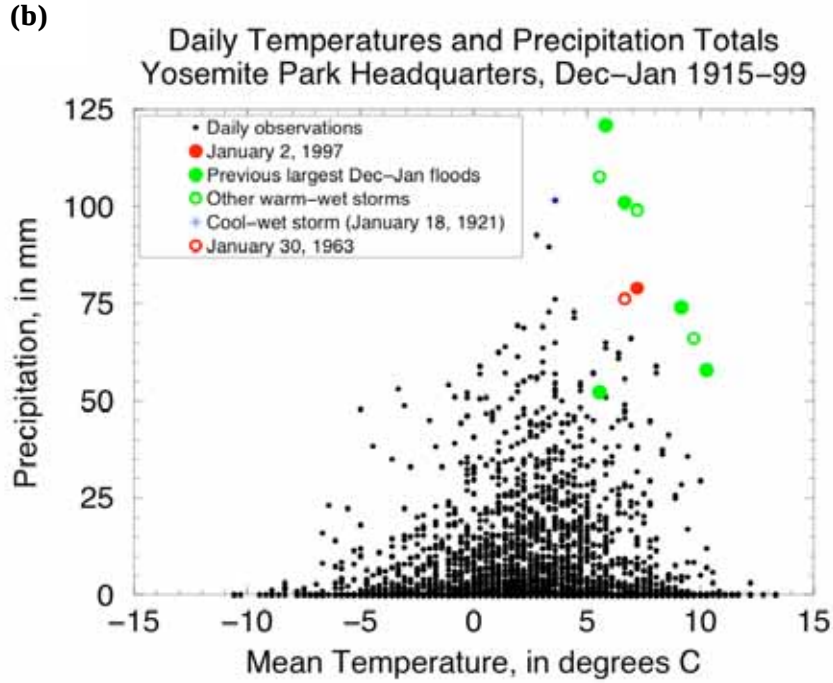

Figure 1. (a) Daily discharges of the Merced River at Happy Isles, Yosemite Valley, 1916–2005, with seasonality of major floods indicated; (b) daily temperatures and precipitation totals in Yosemite Valley during Decembers and Januaries, 1915–1999, with solid dots indicating large floods from panel (a) and open circles and single asterisk indicating storms of similar magnitude that did not yield floods

Yosemite Valley is a particularly helpful place to consider such a flood because it has meteorological and streamflow records that extend back to the 1910s (Figure 1), so that many storms and floods can be analyzed, with little interference by modifications of the local catchments. The New Year 1997 flood inundated large areas in Yosemite Valley, and some $180 million in damages were done to the National Park alone, with damages statewide being many time larger. This flood was one of a handful among historical floods in the Sierra Nevada that are much larger than any others (Figure 1a), all of which have been winter floods and all of which have resulted from very wet and unusually warm storms (solid green dots and red dot, Figure 1b).

Notably, other storms with temperatures and precipitation rates similar to the New Year 1997 storm and these other (solid dots) major floods in Figure 1a have occurred in the historical record, but with little or no resulting flood flows (open circles and asterisk, Figure 1b). Perhaps the most important difference between the flood-generating storms (solid dots) and non-flood-generating storms (open circles) was the saturation of the soils and land surfaces when the various storms arrived. Runoff from large storms that fell on dry soils was reduced, e.g., by the equivalent of 10 or more centimeters of precipitation in the watershed model of Dettinger et al. (2004); runoff from large storms that fell on already wet soils conversely were not as reduced. Figure 2 compares streamflow augmentations from the various large warm storms to precipitation totals in the water year to date, and shows that floods were generated from storms that followed considerable previous precipitation, with resulting wet soils, and were not generated from storms that were essentially first of the wet seasons.

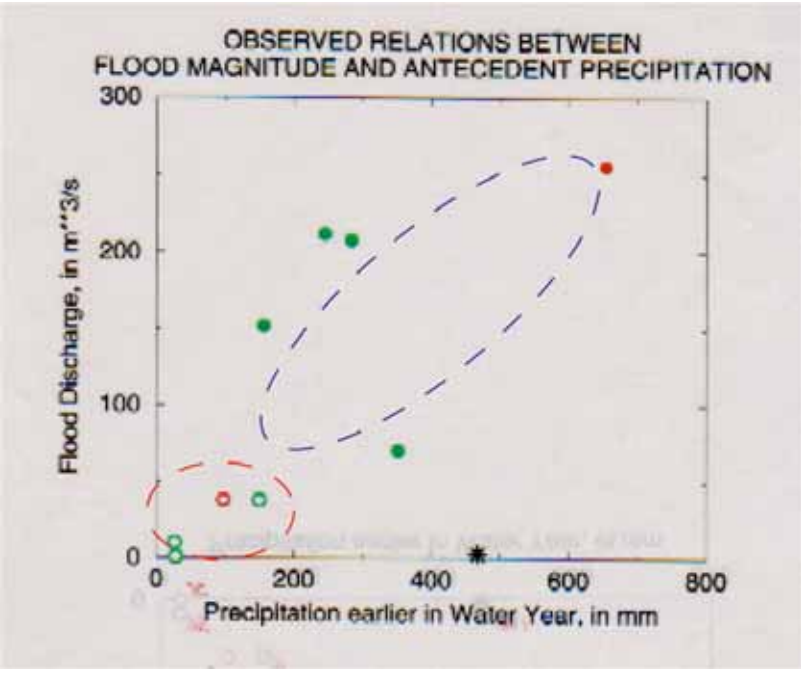

Figure 2. Water-year-to-date precipitation totals and flood discharges in Yosemite Valley associated with selected (symboled) days in Figure 1b; dashed ovals indicate general distribution of discharge episodes with dry antecedent (red) and wet (blue) soils

Although the largest recorded floods have typically been associated with storms with large precipitation totals, storm temperatures also play an important and occasionally dominant role in flood generation. The single asterisk in Figures 1b and 2 represent a storm of January 1921 that was as large as the storms that generated the largest historical floods in Yosemite Valley, but that was too cold to provide much rain and thus too cold to yield high streamflows. More recently, on May 16, 2005, a much smaller storm unleashed a smaller but still significant flood in Yosemite Valley (with daily discharge equal to 4400 cubic feet per second [cfs] or 125 cubic meters per second [m^3/s]). During that storm, precipitation in Yosemite National Park was nowhere measured to be more than 5 centimeters (cm) (Figure 3a), but temperatures were warm enough so that the freezing line was measured (by the Scripps Institution of Technology / United States Geological Survey [USGS] High-Altitude Monitoring Network in the park, Lundquist et al. 2003) to be above 3000 m above sea level (Figure 3b). As a result, rain fell and streams rose over about 85% of the park. The storm followed within about a week of the onset of snowmelt in most of the park (e.g., as recorded by California Department of Water Resources snow pillows at Gin Flat, 2150 m elevation; Tuolumne Meadows, 2620 m; Dana Flat, 2990 m), so that soils were probably already wet. Snow cover was still thick in most of the park (e.g., 85 cm of water content at Gin Flat, 50 cm at Dana Meadows) but rain that fell on the snow did not much change the snowpack water content (Figure 4), that is, rain-driven snowmelt did little to augment the flood flows.

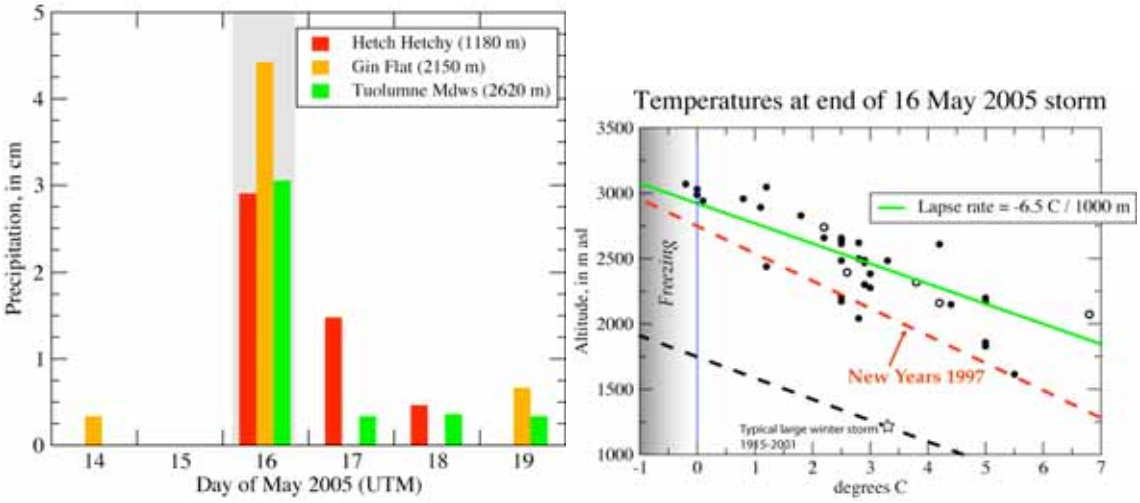

Figure 3. Daily precipitation totals at three precipitation gages in Yosemite National Park, from California Department of Water Resources California Data Exchange Center (left panel) and temperatures at the end (coldest part) of the May 16, 2005, storm from Scripps/USGS Hydroclimatic Monitoring Network in the park, along with long-term average winter-storm temperatures (based on temperatures at Yosemite Valley and assumed -6.5°C (20.3°F)/kilometer (km) temperature lapse rates) and temperatures during New Years 1997 storm (extrapolated from temperatures measured in Yosemite Valley and at Twin Lake, 2440 m elevation) (right panel)

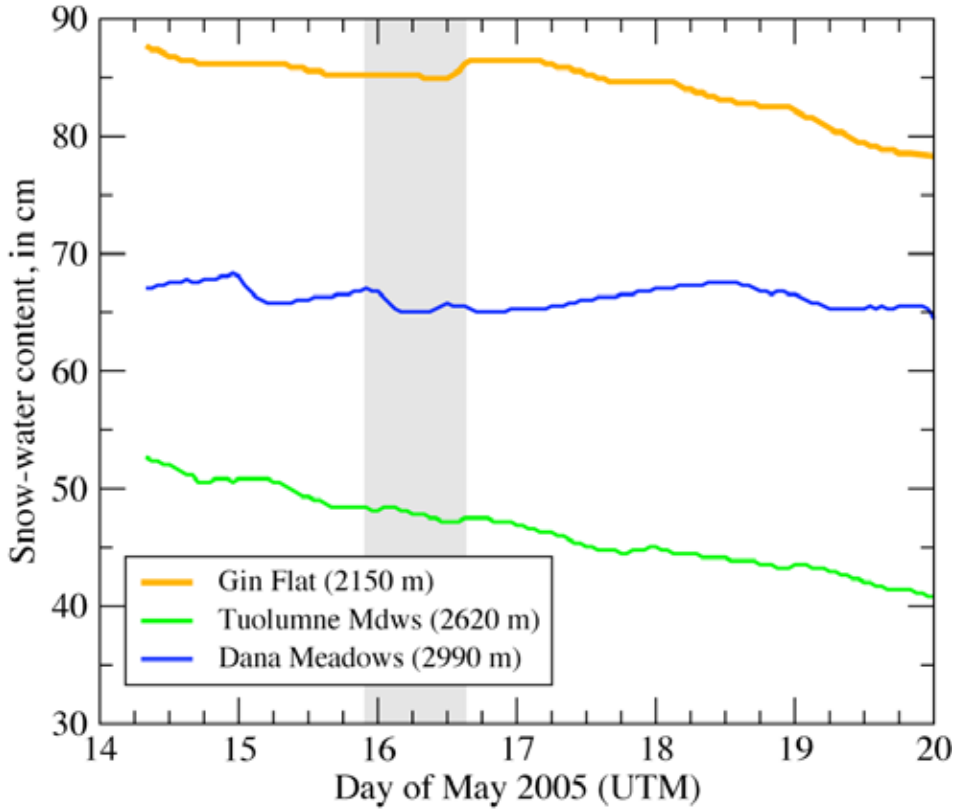

Figure 4. Snow-water contents measured by snow pillows at three locations in Yosemite National Park during May 2005; data from California Department of Water Resources California Data Exchange Center

The flood then was mostly a result of moderate rains over exceptionally large catchment areas. Using the meteorological records from Yosemite Valley, the long-term (since 1915) average percentage of the park that receives rain on stormy days, rather than snow, historically was 15%. On May 16, 2005, more than five times the normal area of the park was receiving rain rather than snow (Figure 5), so that five times the normal area could contribute to rapid runoff and flood generation. We know that rainfed runoff contributed to flood flows across this large fraction of the park, not just from air temperatures during the storm but also because some 20 stream-stage sensors that are part of the Scripps/USGS Hydroclimatic Monitoring Network indicated high stream stages as a result of the storm, to altitudes as high as 3000 m.

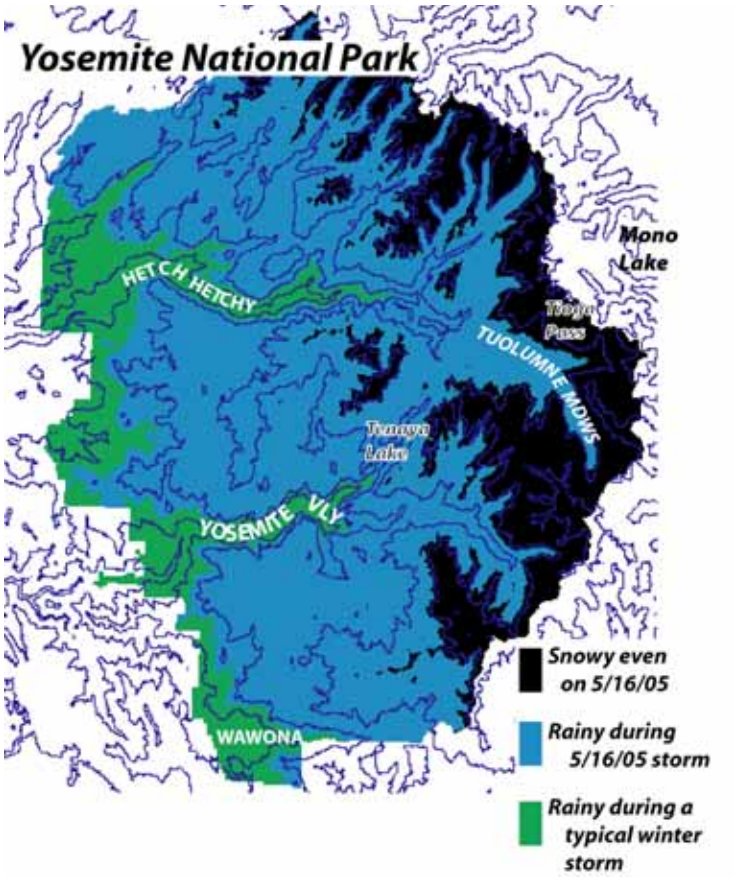

Figure 5. Map of Yosemite National Park, showing areas that typically receive rain in winter storms (green), that received rain on May 16, 2005 (blue), and that received snow on May 16, 2005 (dark blue); the topography of Yosemite National Park is such that its western edge is at a lower altitude (about 1200 m) than its eastern boundary at the Sierra Nevada ridgeline (about 3000 m to 3700 m)

This brief description of storms and floods in the Sierra Nevada provides examples of the importance of how much precipitation a storm delivers, the temperature during the storm, and how wet or dry the soil is before the storm. In a warming world, the statistics of all of these conditions may change. Projections of how large warm storms might change in the twenty-first century are analyzed in the next section. Before that, the potential effects of warming on rainfed contributions to winter floods, the status of winter soil-moisture reservoirs, and the potential for large snowmelt-fed springtime streamflows and floods will be discussed in the remainder of this section.

2.2. Rainfall-Runoff Contributing Areas

The May 16, 2005, flood in Yosemite Valley was an example of how warm storms can deposit rain (instead of snow) over very large catchment areas, increasing the areas contributing runoff to resulting flood flows. The typical temperature "lapse rate," the degree to which temperatures

cool as one moves farther up in altitude, during storms in the Sierra Nevada is about -6.5°C / km (Lundquist and Cayan 2007), so that for each degree warmer that one storm is than another, the dividing line between rainfall and snowfall rises in altitude by about 150 m. In a world in which storms are +3°C (+5.4°F) warmer, snowlines would be about 500 m higher. As shown in the May 16, 2005, flood example, a warm storm can accordingly greatly increase the catchment area contributing rainfall runoff to flood generation.

The extent to which a given amount of warming increases the runoff-contributing areas differs from river to river, depending on the topography of the river basins. For example, Figure 6 compares the fractions of basin areas at various altitudes in four river basins along the western Sierra. The Feather River basin is dominated by catchment areas that are at middle to low altitudes, and thus receives rain on large fractions of the basin in many storms, largely because the basin includes the low altitude Sierra Valley near about 1500 m. The altitude distribution of the American River basin is less peaked at middle altitudes but rises to only modestly higher altitudes than the Feather. The Merced and Kings River basins in the middle and southern Sierra Nevada rise to much higher altitudes and include much smaller low-altitude catchment areas.

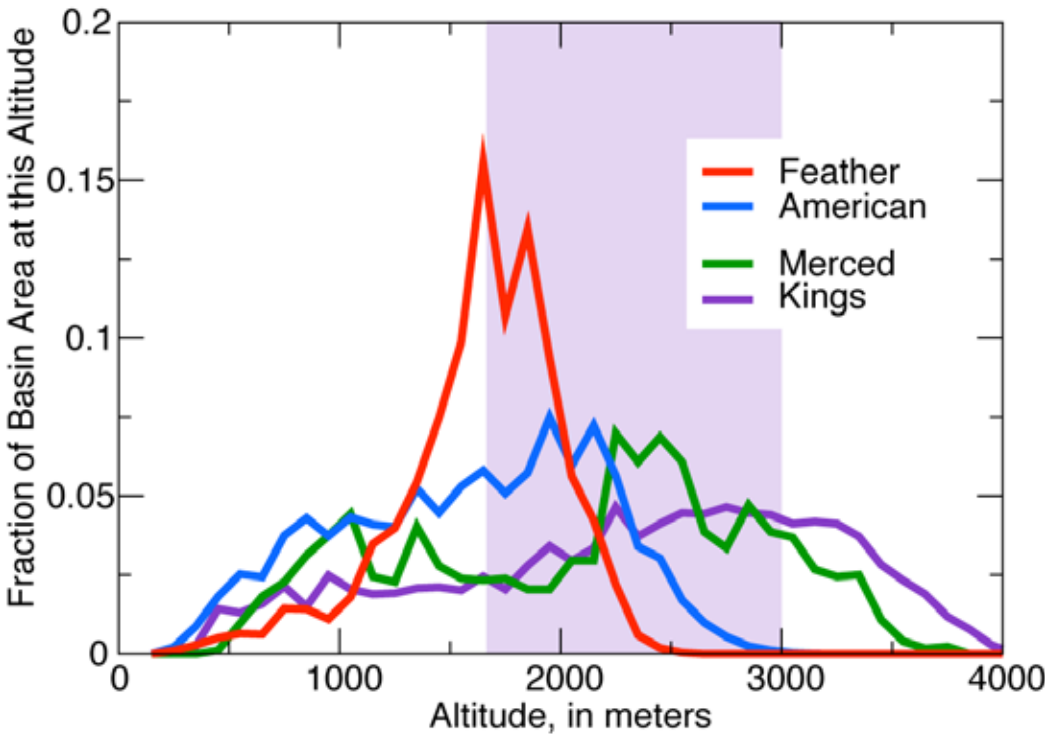

Figure 6. Altitude-area distributions (hypsographs) of four Sierra Nevada river basins. The blue shaded band is roughly the zone within which rain is sometimes deposited under the current climate, but snow is more common.

As a consequence of these altitude distributions, the Feather and American Rivers very likely have received rainfall, rather than snowfall, up to their highest areas in at least some historical storms. The Merced and Kings Rivers, in contrast, only rarely if ever have received rainfall from

winter storms to their highest ramparts historically. In a river that historically has received rain throughout its catchment, additional warming alone (without changes in precipitation rates during storms) may (a) increase the frequency of storms that unleash these rainiest of conditions or (b) in principle, may increase the number of occasions when rain falls on snow to augment flood generation. Chances are that, in such basins, flood frequencies can increase in response to warming conditions, but that increases in the magnitudes of the largest floods may depend almost entirely on what happens to the amounts of precipitation dropped by storms. By contrast, in basins where rain has never reached the entire catchment in historical storms, warming alone can also result in storms where much larger-than-historical areas contribute to flood generation by receiving rains. Resulting rainfed floods in such basins can be much larger than any historical floods, without any real change in the magnitude of storms.

To illustrate this difference more concretely, daily temperature series at Yosemite Valley (for the Merced River) and at Central Sierra Snow Lab (for the American River) were analyzed for all wet days (not just winter storms) during their respective periods of meteorological record. For each wet day, the altitude of snowline was broadly estimated by extrapolating temperatures upward or downward until the freezing level was reached, assuming that a -6.5°C/km temperature lapse rate prevailed on the wet days studied. The resulting estimated freezing altitude was then compared to the hypsographs (Figure 6) for the two basins to estimate, day by day, what fraction of the basins were above or below freezing; receiving rain or snow respectively. The historical numbers of storms that these estimates indicate deposited rain on various fractions of the two river basins are indicated by the black curves in Figure 7. The curves in the two panels are quite different from each other, with the Merced River numbers of rainy days declining essentially to zero when the basin-area threshold (receiving rain) is above about half the basin, whereas the numbers for the America River are still well above zero (closer to 25%) for the entire basin receiving some rain.

The red curves in Figure 7 show the corresponding numbers of storms when the calculations are redone, but with the entire historical temperature record increased by +3°C. Under this hypothetical climate change, the numbers of storms that deposit rain on nearly the entire Merced River basin increase dramatically; e.g., from effectively never, historically, to about 3% of the storms under the imposed warmer conditions for rain reaching 80% of the basin. In the American River basin, such a warming would increase the number of storms depositing rain on as much as 80% of the basin, from about 40% of storms historically to about 75% with the imposed warming. This is a marked increase in the number of such storms in the American, indicating an increasing frequency of storms that create strongly rainfed flood potentials, but in the Merced, the change is from never having seen such storms and floods to, under warming, seeing them upon occasion.

A broad interpretation of these considerations is that the higher, southern parts of the Sierra Nevada may respond to warming by increasing both frequencies and, potentially, magnitudes of future floods. Under the same assumptions and considerations, the northern Sierra may experience more floods, potentially many more, but not necessarily many much-larger floods.

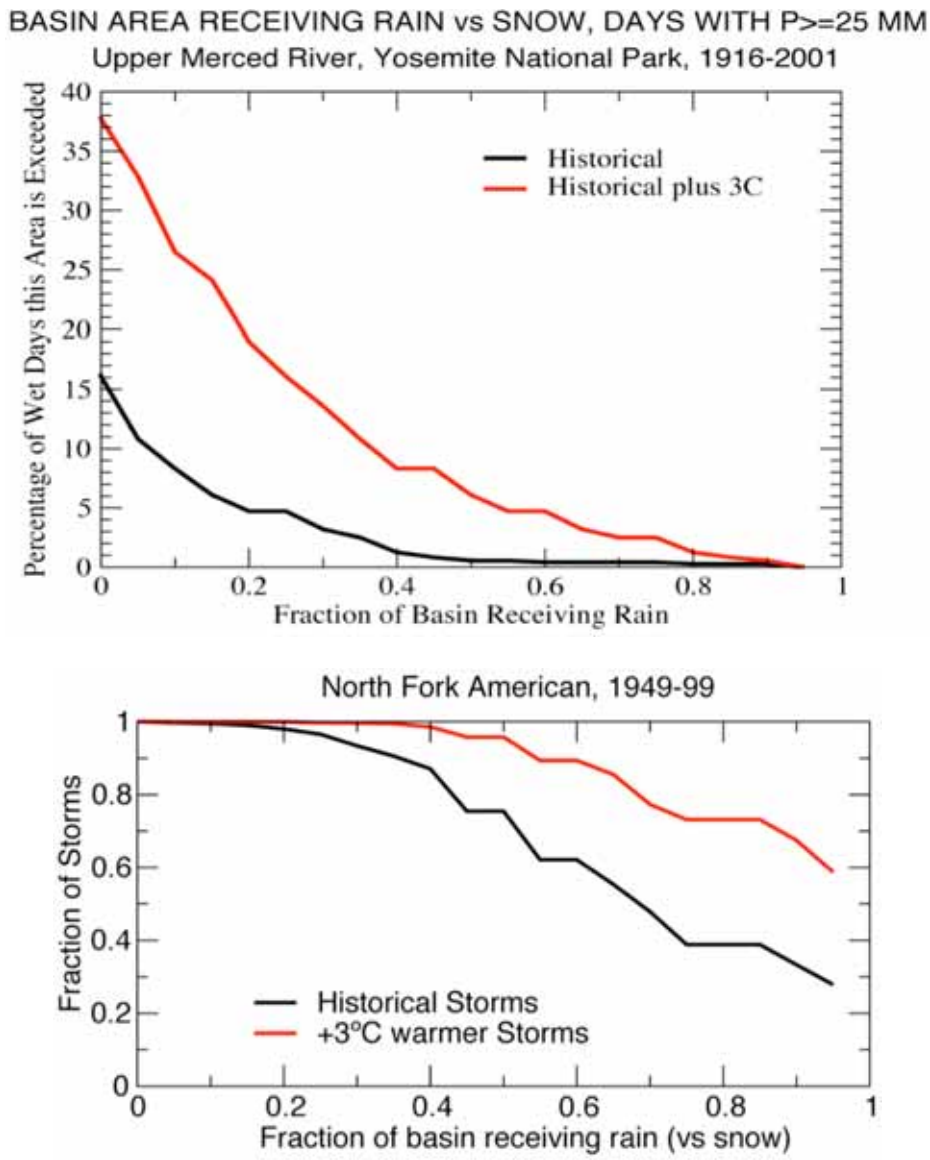

Figure 7. Fractions of historical (black curves) and warmer (red curves) wet days on which rain might be deposited on various fractions of the Merced River basin (above Yosemite Valley, top panel) and of the North Fork American River basin (above North Fork Dam, bottom panel). The warmer scenarios are simply the historical record from each, augmented by a uniform +3°C (+5.4°F) warming. The method used to estimate these fractions is described in text.

2.3. Rain on Snow

The overall effects that warming trends will have on the incidence of rain-on-snow and rain-on-snow augmentations to flooding in California remain difficult to discern. Warming may generally reduce the amount of snow upon which rain may fall by decreasing the amount of snow that falls, by raising snow lines generally, and by melting snow before rain falls. In contrast, though, as long as snowpacks form, warming may tend to increase the numbers and

reaches of rainy storms and may yield ever-warmer rains to melt the snows upon which they fall. Most often, important rain-on-snow melting events occur when a cold storm deposits snow at low altitudes, followed by a warm storm that deposits warm rains on these, and higher, snow fields. Methods for reliably identifying and counting such cold-warm storm sequences in global-climate projections are not well developed yet, and so the future of these events is largely unknown. Given these several competing influences, and the fact that climate models (and most of the hydrologic models used for state-scale simulations of climate-change impacts) are too coarsely resolved to confidently represent the sequences of events and outcomes associated with rain on snow, at present the future role of rain-on-snow events in twenty-first century flood regimes remain highly uncertain and history may be the best guide at present.

Historically McCabe et al. (2007) have shown that, with warming in the western United States, the occurrence of rain-on-snow events have declined at lowest sites and have increased at higher sites. The decreasing numbers of low-altitude rain-on-snow events reflect declining periods of time when snow is on the ground and available to be rained upon. The increasing frequency of rain on snow at higher altitudes probably reflects increasing tendencies toward storms with unusually high snowlines and unusually broad rainy areas in many parts of the West (e.g., Knowles et al. 2006).

This combination of trends at high and low altitudes probably corresponds to reductions in the risks of major rain-on-snow contributions to floods in the west in recent decades. The thermodynamics of melting snow (to contribute much to floods) by depositing rain on the snowfields is such that generation of large amounts of melt water is easiest (and most common) at lower altitudes. To melt a gram of snow, about 330 joules of heat must be added; to cool a gram of rainwater by 1°C (1.8°F), about 4 joules of heat must be extracted (Rogers and Yau 1989). Because of this, a gram of rain can melt about 1/80 of a gram of snow for each degree that the rainwater is cooled in the process. Even a gram of rain at +10°C (+50°F) might therefore only result in the melting of about 1/8 of a gram of snow, so that rain on snow is typically only a modest amplification of runoff contributions from the rain itself.

Detailed measurements of rain-on-snow snowmelt heat balances by Marks et al. (1998) and Wondzell and King (2003) indicated that heat from rain does little to melt snow and that condensation of water vapor onto the snow has a larger effect. More recently, Mazurkiewicz et al. (2008) have evaluated longer records (including more episodes) to find that, perhaps, radiation effects are even larger contributions to snowmelt during these episodes. Each of these studies also found that the water liberated by melt in these events is a relatively small fraction of the total (e.g., < 35% in Mazurkeiwicz et al. 2008). Common wisdom also notes that rain on snow can liberate extra water for runoff when it softens and weights down snowpacks on steep surfaces so that they break loose and slide into waterways. None of these processes are well represented in available climate or hydrologic models, so that, once again, more research will be required to predict the future contributions of rain on snow to California's floods.

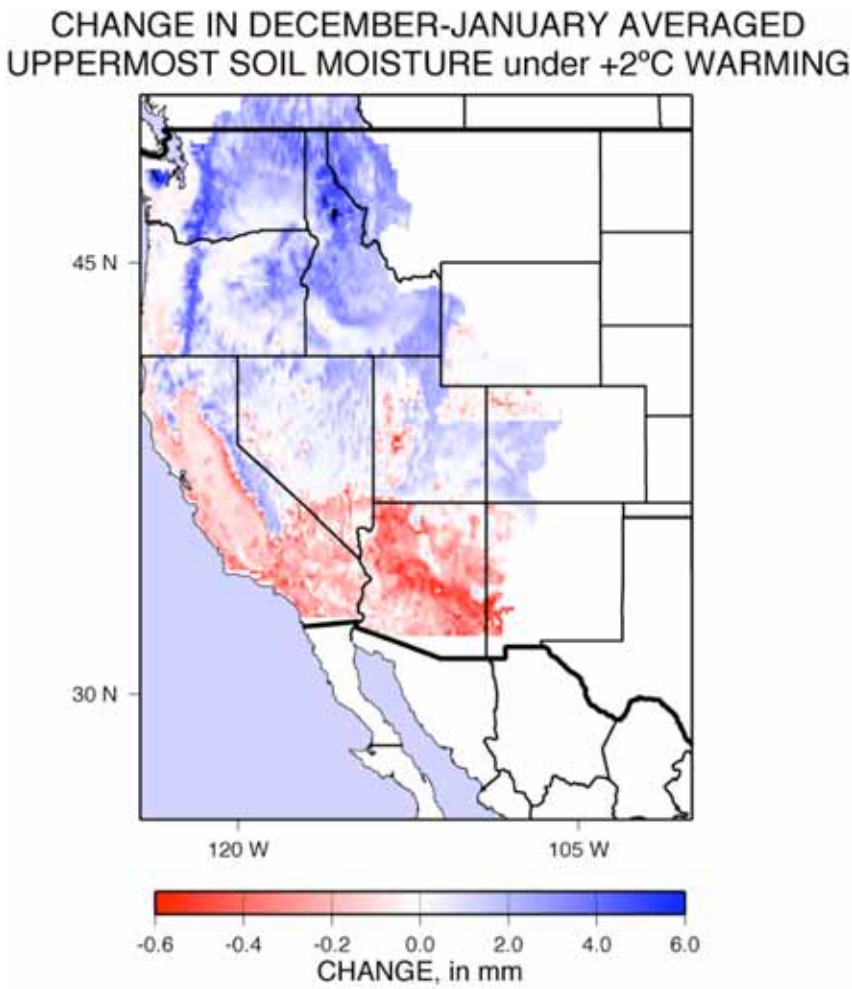

Figure 8. Simulated differences in soil-moisture contents in the upper 5 cm of soil column between a simulation of hydrologic variability driven by historical meteorology, Decembers and Januaries 1950–1999, and a similar simulation but with temperatures uniformly elevated by +2°C (+3.6°F); simulations were made with the Variable Infiltration Capacity (VIC) land-surface hydrology model on a 12-km grid. Notice that color bar representing reduction in soil moisture with warming (reds) is expanded by a factor of ten relative to the color bar for soil-moisture increases (blues).

2.4. Antecedent Soil Moisture

As far as the direct effects of warming on winter and spring flood potentials go, warming might generally be expected to increase the potential for evaporation, sublimation, and transpiration from the soils of mountain catchments in ways that could tend to reduce the size of future floods. If soils are so dry at the beginning of a storm that the first five or ten centimeters of rain go to replenishing them, storms must be that much larger in order to generate floods. However, as long as there is generally some snow on the ground in California's mountains, warming is likely to increase the number of occasions when the snow will melt even in mid-winter. During the critical winter season for California floods, the resulting "snowmelt drizzle" has been

simulated in several different hydrologic modeling systems in the Sierra Nevada; e.g., in the Precipitation-Runoff Modeling System models of the Merced, American, and Carson Rivers (Dettinger et al. 2004); in the Variable Infiltration Capacity (VIC) (Liang et al. 1994) model; and in the Bay-Delta Watershed Model (BDWM) (Knowles and Cayan 2004). The difference between winter soil-moisture contents in a VIC simulation of the hydrology of the West under historical meteorological conditions and under the same conditions except with a +3°C uniform warming imposed are shown in Figure 8. In the northern, snowier two-thirds of the simulated region, including the Sierra Nevada, winter soil-moisture contents increase in response to warming. Such wetter winter conditions would not discourage the enhancement of winter floods in the Sierra Nevada, and if anything, might increase the potential for more flooding as a result of warming.

2.5. Synchronous Springtime Snowmelt

Finally Lundquist et al. (2004) described a class of spring snowmelt conditions in the Sierra Nevada in which the temperature transition from cold winter conditions to warmer spring conditions is rapid enough so that most altitudes rise above freezing levels within a day or two of each other. Under these circumstances, snow fields at locations ranging from middle to highest altitudes begin to melt within a day or two of each other, or "synchronously." Such spring snowmelt seasons were observed by the Scripps/USGS Hydroclimatic Monitoring Network in the high country of Yosemite National Park and have been inferred (from older streamflow, snow, and meteorological records) to have occurred infrequently in the historical period, only about eight times in 87 years. Recent synchronous springs have not occurred in particularly wet years (e.g., 1999 and 2002). However, because snowmelt is contributed from the entire range of altitude zones synchronously, if snowmelt is strong in one of these springs, the resulting springtime flows can be large. Lundquist et al. (2004) note an instance of such synchronized snowmelt in Colorado in a wet year (1983) that led to springtime flooding.

As California's climate warms, the opportunities for such synchronized springs in the Sierra Nevada may increase as temperatures leading up to spring snowmelt hover ever closer to freezing throughout the range. If so, then the extent to which warming actually increases the number or magnitude of spring snowmelt floods will depend on whether synchronization (which would contribute toward flooding) is a larger effect than will be the warming-induced depletion of the state's springtime snowpacks, which must be large if floods are to be developed. At present, the likely outcome of that competition is uncertain.

3.0 Projections of Future Atmospheric-River Storms

Although warming may be expected to alter flood regimes in many snowfed settings, the prospect of changes in California's storm types, frequencies, or magnitudes provides more direct and pervasive opportunities for change. In this section, projections of the future of some of the most important storms, in terms of flood risk, will be reviewed and discussed. Probably the most dangerous storms in California have been warm and wet storms that historically have struck California in winter, producing intense rains over large areas and unleashing many of the state's largest floods. The most commonly recognized of these storms have been described as "pineapple express" storms because of the clear way that they appear (in weather satellite and other imagery, e.g., Figure 9) to draw warm, moist air from the tropics near Hawaii northeastward into California (Weaver 1962; Dettinger 2004). Historically intense versions of

these storms have occurred on an average of about four days per year (Dettinger 2004). Many of the largest floods in the past 100 years (at least) have occurred in response to the large volumes of rain that these storms have dropped on the state (Dettinger 2004; Ralph et al. 2006; Neiman et al. 2008a).

More recently, studies have shown that "pineapple express" storms in California are just one version of a more common feature of the midlatitude atmospheric arm of the hydrologic cycle. It has been determined that about 90% of all the water vapor transported toward the poles across the midlatitudes is transported within narrow, intense filamentary bands of moist air, called atmospheric rivers (AR) (Zhu and Newell 1998), that together typically span less than about 10% of the circumference of the globe at any given time. The long band of bright colors (high water vapor amounts) in Figure 9 between roughly Hawaii and central California in the top panel of Figure 9 is the AR associated with the New Years' 1997 storm and gives a sense of the scope and scale of these features, as do other similar filamentary features in the southern hemisphere in that image; the other panels show other ways of visualizing the same episode. Investigations by Ralph et al. (2004, 2005, 2006), Bao et al. (2006), Neiman et al. (2008a), and others have shown that, as they approach the west coast of North America, these ARs are typically 2000 or more kilometers long and only several hundred kilometers wide (Ralph et al. 2006). The air column within a typical AR will contain more than 2 cm of water vapor, with most of that vapor contained in the first 2.5 km above the sea surface and with a jet of intense and moist winds centered near about 2 km above the surface (Neiman et al. 2008a). When the AR is oriented so that these intense winds carry their moist air directly up and over the mountains of California (that is, in directions nearly perpendicular and upslope into the mountain ranges), intense storms of orographically enhanced precipitation result (Neiman et al. 2002; Andrews et al. 2004; Dettinger et al. 2005).

Ralph et al. (2006) recently noted that all "declared" floods on the Russian River near Guerneville (in the Coastal Range north of San Francisco) during the past 10 years have occurred within a day of the arrival of one of these ARs. Dettinger (2004) showed that, during the past 50+ years, flows in the Merced River near Yosemite Valley have typically risen by about an order of magnitude more following the pineapple express form of ARs than following other winter storms. Less formally, all of the major winter floods on the Carson River in the eastern Sierra Nevada in the past 50 years have also been associated with pineapple-express storms (as determined by comparing the flood chronologies of Jeton (2006), to updated pineapple-express chronologies from Dettinger (2005).

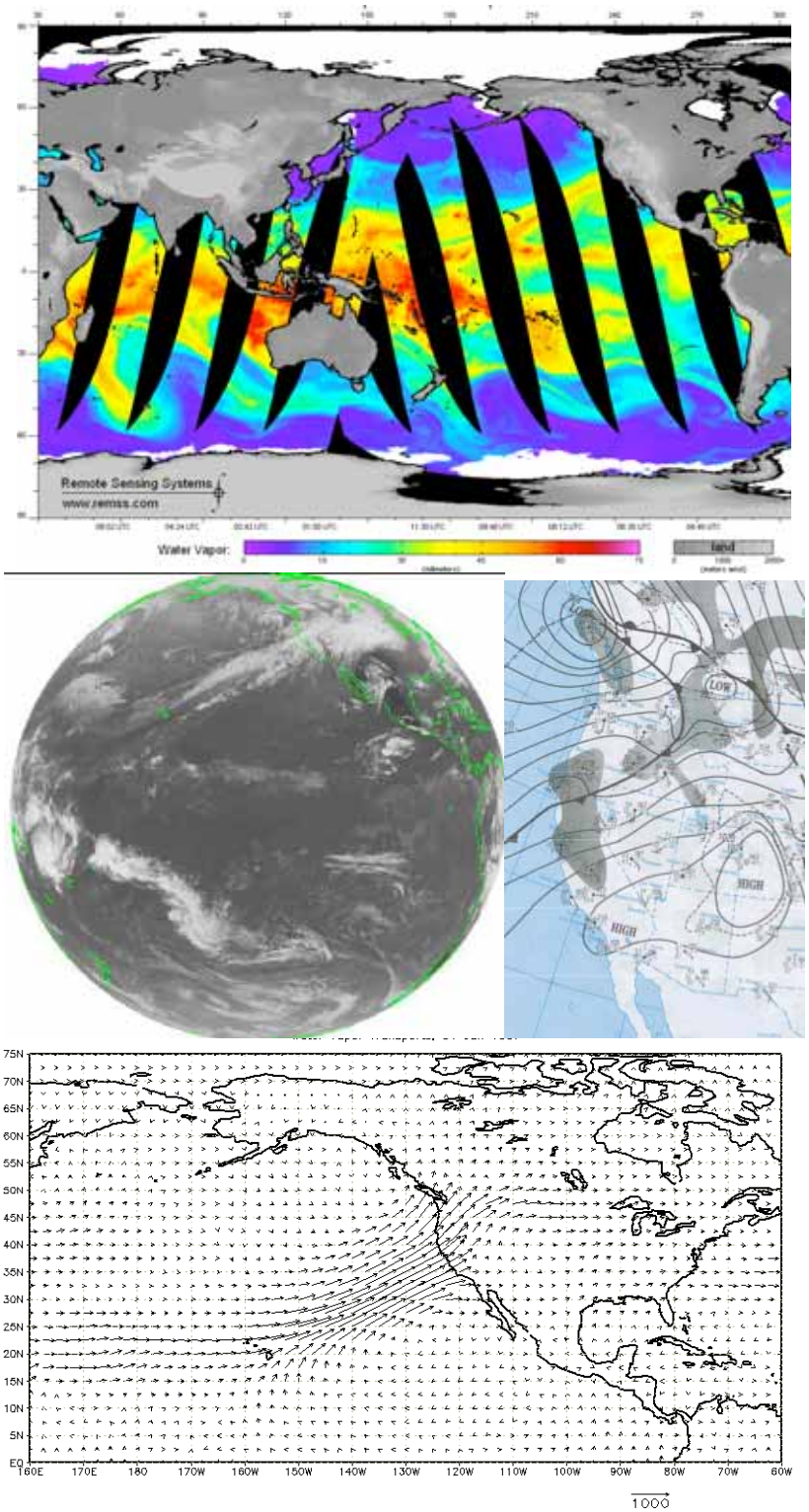

Figure 9. (Top) Special Sensor Microwave/Imager (SSM/I) integrated water vapor imagery from GMT morning on 2 January 1997. (Middle left) Infrared weather-satellite imagery of the Pacific Ocean basin (GOES-West) from 1800 hours GMT on 1 January 1997, and (middle right) a corresponding daily weather map. (Bottom) Vertically

integrated water-vapor transport directions and relative rates. The arrow at the bottom indicates the length of a 1000 kg/m/s transport.

Thus AR storms have historically been the source of most of the largest floods in California, and an evaluation of the future of floods in California must ultimately attempt to understand the future of these storms, specifically the future of their frequency of occurrence and of their intensities at landfall along the California coast.

Intense pineapple express storms can be identified in daily general-circulation model (GCM)-scale atmospheric fields by tracing back to sources of intense water vapor transport plumes to determine which begin in the subtropics or tropics near Hawaii (Dettinger 2004). However, this can be a cumbersome algorithm to apply to current projections of climate change, because of the large fields that must be manipulated and because some of the necessary variables are not available from most of the Intergovernmental Panel on Climate Change (IPCC) GCMs at daily resolutions. Thus a more locally based strategy for detecting precipitation-rich AR-type storms along the California coast, designed and described by Neiman et al. (in press), is applied to climate-change projections from IPCC GCMs in this paper. The GCM-friendly AR-detection approach is to calculate the vertically integrated water vapor (IWV) in the atmosphere and the wind speed and direction at the 925 millibar (mb) pressure level (about 1 km above the surface) above a GCM grid cell just offshore from the central California coast. In this study, these variables were determined for each day from the periods 1961–2000, 2046–2065, and 2081–2100, and, in a GCM-based parallel of Neiman et al.'s (in press) primary application of the method, to date, to the San Francisco coastal region, for a grid cell offshore from San Jose. The wind directions are evaluated to determine the component of wind that is directly upslope on the mountain ranges upon which the ARs are impinging, and when the upslope wind component is greater than 10 m/s while the integrated water vapor is greater than 2.5 cm (in this study), an AR storm is believed to be occurring. In nature, all storms that dropped more than 10 millimeters (mm)/hour of precipitation at the National Oceanic and Atmospheric Administration (NOAA) Cazadero meteorological station since 1998 have met roughly these criteria.

Applying the criteria above to historical and future climate simulations by seven IPCC GCMs allows us to compare the frequencies and magnitudes of AR storms arriving in California in the models under simulated historical and climate-changed conditions. Through this analysis, we begin to determine whether these particularly dangerous storms, and their attendant flood risks, will increase or decrease under the influence of increasing greenhouse gas concentrations in the global atmosphere during the twenty-first century.

For example, the plot of daily IWV and upslope 925-mb wind speeds as simulated by a particular climate model (the Geophysical Fluid Dynamics Laboratory [GFDL] CM2.1) under historical (blue dots) and future twenty-first century (red dots) conditions is shown in Figure 10a. Conditions on a relatively few historical December–February days fall in the upper right quadrant of this figure, where IWV > 2.5 cm and upslope wind > 10 cm, and the number of such days increases slightly as the climate evolves under the influence of increasing greenhouse gas concentrations due to the A2 emissions scenario analyzed here (Figure 10b). The slight increase in number of winter days that meet the historical AR criteria (in this particular model) is a suggestion that opportunities for a major AR storm with potentially attendant winter flooding might increase with climate warming. In this model, the upslope winds slacken notably (red

dots are generally farther left on Figure 10a than blue dots), and this almost compensates for the tendency of the IWVs to be larger, so that only marginally more days appear in the "extreme-precipitation" upper right quadrant. By analyzing such figures from several models and by analyzing the corresponding projected weather conditions that prevail on the days that meet the ARs criteria, key factors that will determine the intensity and risks associated with individual AR events can be inferred. In order to develop a sense of the extent to which resulting inferences depend on the particular climate model considered, in this investigation, statistics of ARs from seven different climate models will be evaluated. All AR statistics shown here will either be from IPCC simulations of historical climate (20c3m) conditions or from IPCC future (A2 emissions) conditions, where the A2 emissions are a scenario in which greenhouse gas emissions grow and, indeed, accelerate quickly throughout the twenty-first century. The A2 scenario was investigated here because it provides the most severe climate changes among the scenarios for which climate projections are commonly available.

Figure 11 shows the numbers of December–February days during the 1961–2000, 2046–2065, and 2081–2100 periods that have IWV > 2.5 cm and upslope winds > 10 m/s, in each of seven GCMs and in the observations-based National Center for Atmospheric Research-National Centers for Environmental Prediction (NCAR-NCEP) Reanalysis data set (Kalnay et al. 1996). The open (Reanalysis) circles represent real-world analogs to the simulated fields from the seven GCMs, and the number of Reanalysis AR episodes is on average lower than the numbers simulated by most of the GCMs (excepting the two Japanese models, see caption of Table 1 for list of models analyzed). Nonetheless, the range and general distribution of numbers of AR days per winter are not so different from the GCM counts as to preclude evaluations of the projected changes in the ensemble of GCM projections.

Numbers of AR days during the twenty-first century increase in most of the GCMs (compared to their respective historical counts), but with most of those increases occurring as increased numbers of winters with many AR days and decreased numbers of winters with very few AR days (Table 1). That is, most models simulate more winters with many opportunities for AR storms and floods, and fewer winters with few opportunities, under the influence of increasing greenhouse gases and warming. Changes in the frequency of these "extreme" winters are more notable than corresponding changes in the long-term mean numbers of AR storms.

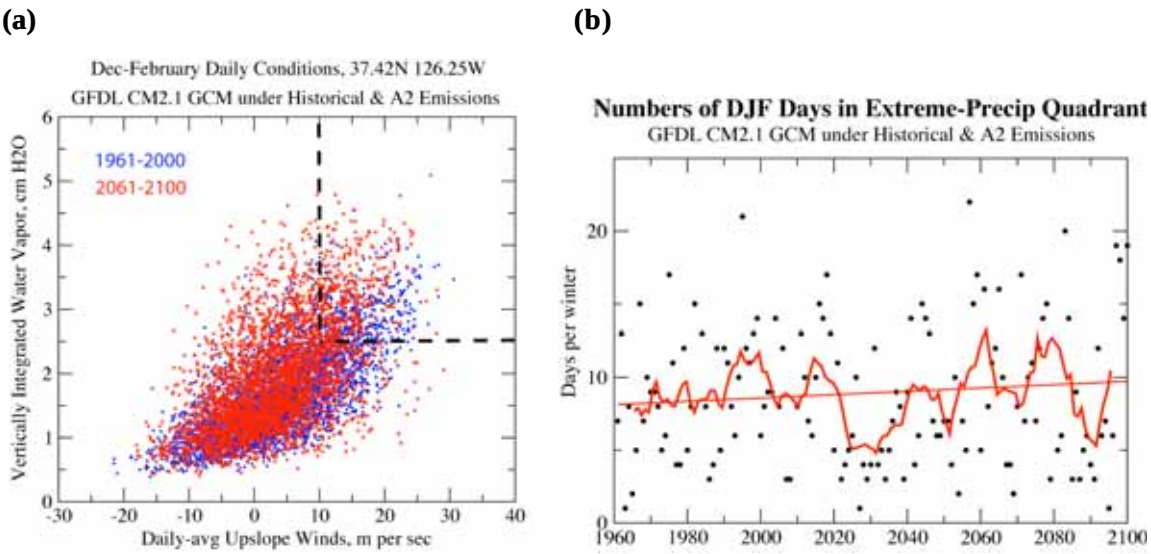

Figure 10. (a) Plot of daily December–February integrated water vapor (IWV) and upslope wind values from GFDL CM2.1 climate model, and (b) numbers of days per winter falling into the upper right quadrant of that plot, under evolving 20th- and 21st-century climate changes with A2 greenhouse gas emissions

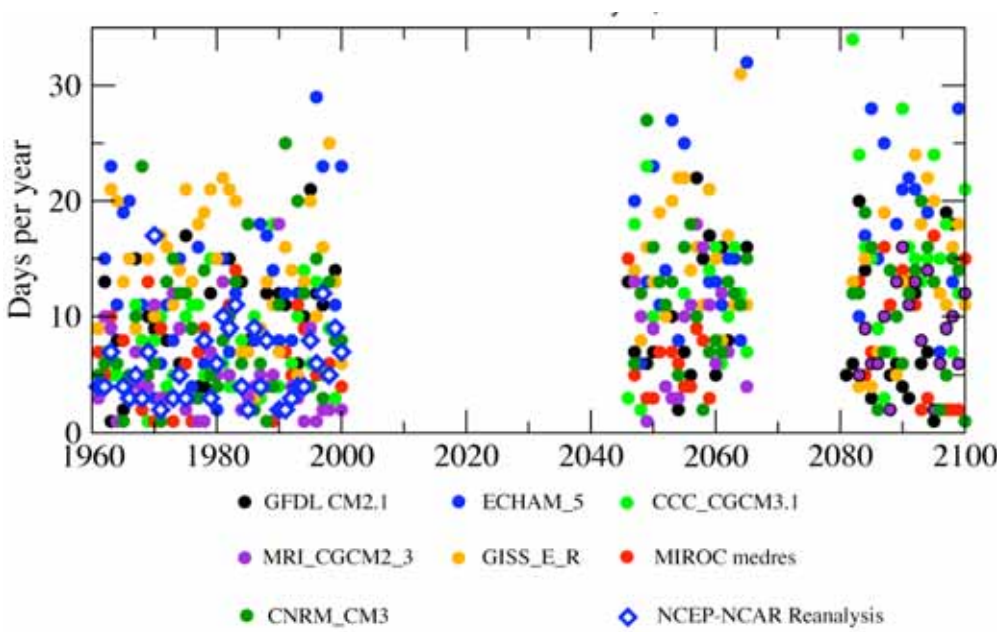

Figure 11. Numbers of December–February days per year in the upper-right quadrant of Figure 10a, for seven climate models and the NCAR-NCEP Reanalysis data fields; 21st century counts are from projections made in response to A2 emissions scenarios

Table 1. Counts of December–February days with IWV > 2.5 cm and upslope winds > 10 m/s in an ensemble of projections of climate change under an historical and A2-future emissions scenario from seven GCMs and in the NCAR-NCEP historical Reanalysis dataset; GCMs are the CCC CGCM3.1 (Canadian), CNRM CM3 (French), ECHAM 5 (German), GFDL CM2.1 (US), GISS Er (US), MIROC medium-resolution (Japanese), and MRI CGCM2.3 (Japanese) climate models

	Mean #/yr	# yrs < 5 AR days (%)	# yrs > 10 AR days (%)	# yrs > 15 AR days (%)	# yrs > 20 AR days (%)
1961–1980	**8.5 days**	**25**	**38**	**16**	**5**
1981–2000	**9.0**	**27**	**40**	**16**	**8**
2046–2065	**11.6**	**12**	**63**	**28**	**10**
2081–2100	**11.7**	**16**	**62**	**32**	**12**
Reanalysis 1961–2000	**5.8**	**42**	**10**	**3**	**0**

To be more specific, Table 2 shows how the numbers of AR days per winter change through time on a model-by-model basis, as indicated by linear regressions of the AR-day counts from all available winters (1961–2000, 2046–2065, 2081–2100) versus year. AR-day counts increase in five of the seven models and counts in the remaining models remain at historical levels. The projected numbers of AR days in the twenty-first century average (across the ensemble of models) about +2.5 days, or about 30%, more by end of century. Thus opportunities for winter-flood generating storms in central California are generally (but not unanimously) projected to increase in frequency in response to the growing perturbations of the climate system by increased greenhouse gases in the atmosphere.

Table 2. Trends in numbers of AR days / 100 years from seven climate models, with trends that rise to statistical significance at 95% level highlighted in boldface, and with (*) the trend in the CNRM model only just missing the 95% significance level

	Change in # AR days / 100 yr	R^2 of trend fit (%)
CCC	**+7.2 days**	**30**
CNRM	+2.4	4 *
ECHAM	**+4.5**	**10**
GFDL	+0.4	0.2
GISS	+0.3	0
MIROC	**+2.2**	**7**
MRI	**+3.6**	**15**

The intensity and characteristics of these simulated (and observed) AR events may also be evaluated, in order to determine how AR episodes themselves may evolve in the twenty-first century. Figures 12 and 13 compare distributions of IWV values and upslope wind speeds on

AR days under the historical and projected-future climates from each of the seven models. Integrated water vapor on AR days increases in all of the models, as do the numbers of AR days with IWV values greater than about 3.5 cm to 4 cm. In the real world, AR days with such high IWV values have been associated with the very largest storms (Neiman et al. 2008b) and thus the increases at the rightmost edges of the histograms of Figure 12 suggest rather ominous changes in the amount of precipitation that many of the projected AR days may deliver in the future.

On the other hand, the histograms of upslope wind speeds in Figure 13 indicate that, in all of the models except perhaps CCC, the upslope components of the winds transporting the additional water vapor tend to weaken as the twenty-first century proceeds. These weaker upslope winds will tend to work against the increased water vapor to reduce the orographic precipitation totals that the ARs might deliver. Indeed, the product of the upslope wind times the IWV gives an approximate sense of the water vapor delivered and available to be rained out of the AR storms as they pass over California's mountains. Figure 14 shows the distributions of this "intensity" product for each of the models, with the strong suggestion that in most models, although the numbers of AR days increase, the distributions of their overall (product) intensities may not change as much. Table 3 shows the regressed trends for these intensities on a model-by-model basis, indicating that three of the seven models produce statistically significant increasing trends in the winter-average intensities of AR circulations, two more models yield increases that are not statistically significant, and season-average intensities in the remaining two models remain more or less the same. Even in the models that produce significant trends in AR intensity, the changes are not (on average) more than about 10%, which might be interpreted to translate into an average of not much more than about +10% more rain from future AR storms. Nonetheless, notice that more-than-historical numbers of ARs fall into the most intense tails of the projected distributions (Figure 14) from all seven GCMs. This tendency toward the occasional future occurrence of ARs that are more intense than witnessed historically is an indication that, under projected climate changes, occasional AR storms are likely to be more intense than has been experienced historically so the largest AR-related storms in the future may be larger than any historical storms.

Table 3. Trends in intensity (IWV * upslope wind speed) of AR days / 100 years from seven climate models, with trends that rise to statistical significance at 95% level highlighted in boldface, and with (*) the trend in MRI only just missing 95% significance level

	Change / 100 yr	% change / 100 yr	R^2 (%)
CCC	**+5.7 cm H_2O * m/s**	**+11**	**12**
CNRM	**+4.0**	**+ 9**	**8**
ECHAM	**+3.8**	**+ 7**	**6**
GFDL	+0.1	0	0
GISS	+1.6	+ 4	3
MIROC	-0.3	- 1	0
MRI	+2.1	+ 5	3 *

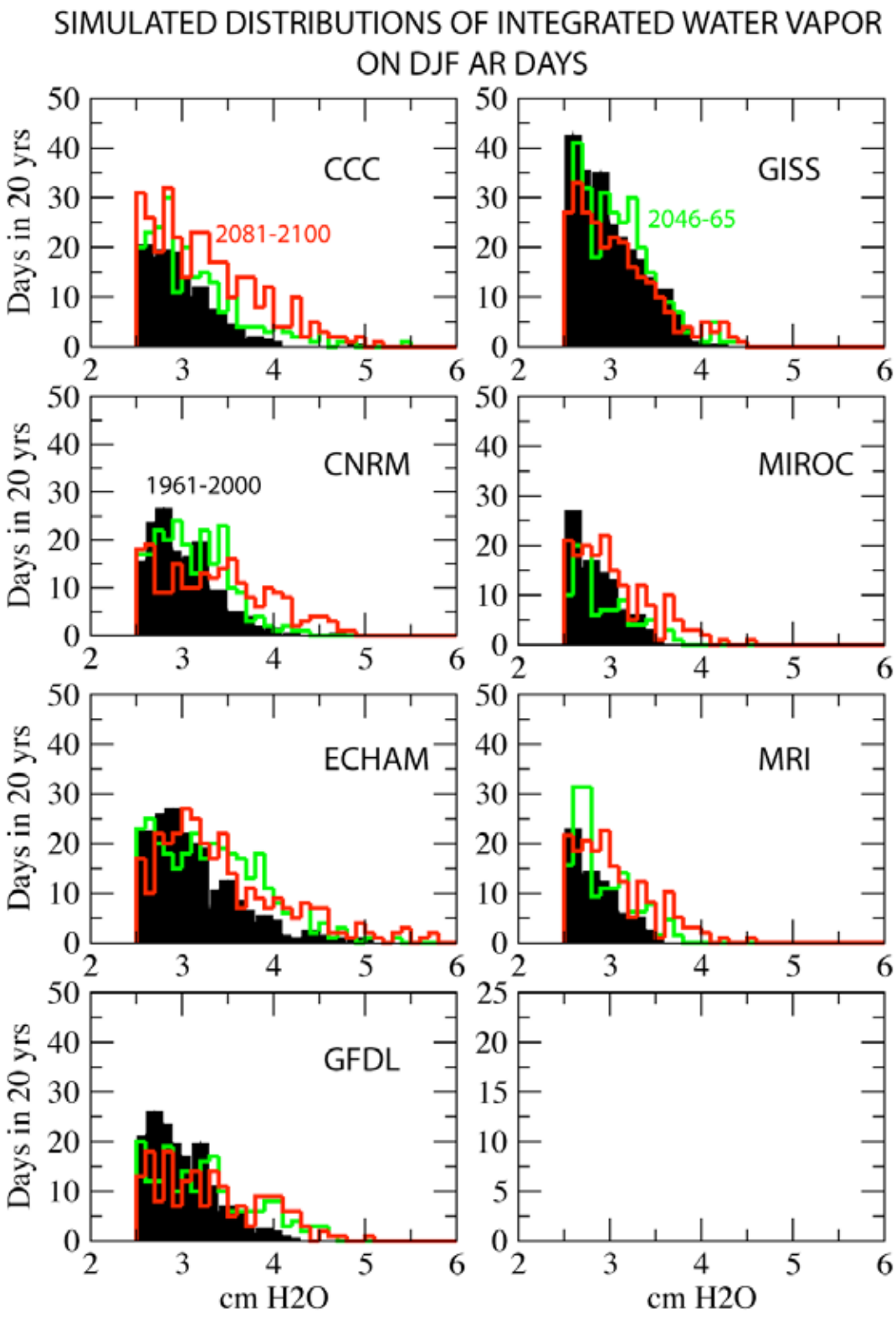

Figure 12. Histograms of simulated historical (20c3m, black) and future (A2, green and red) distributions of integrated water vapor values associated with AR-days in seven climate models

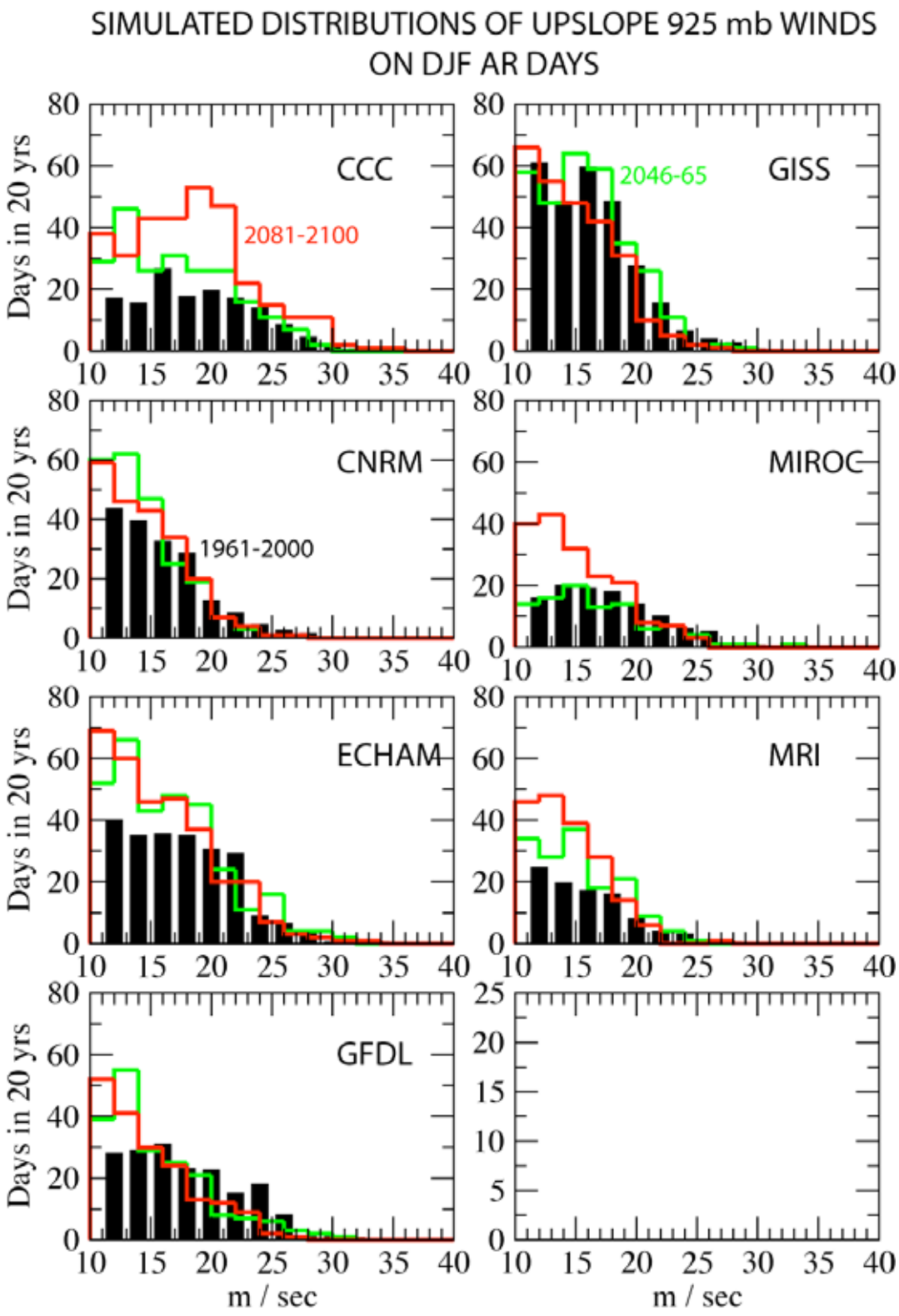

Figure 13. Same as Figure 12, except for upslope winds on AR days

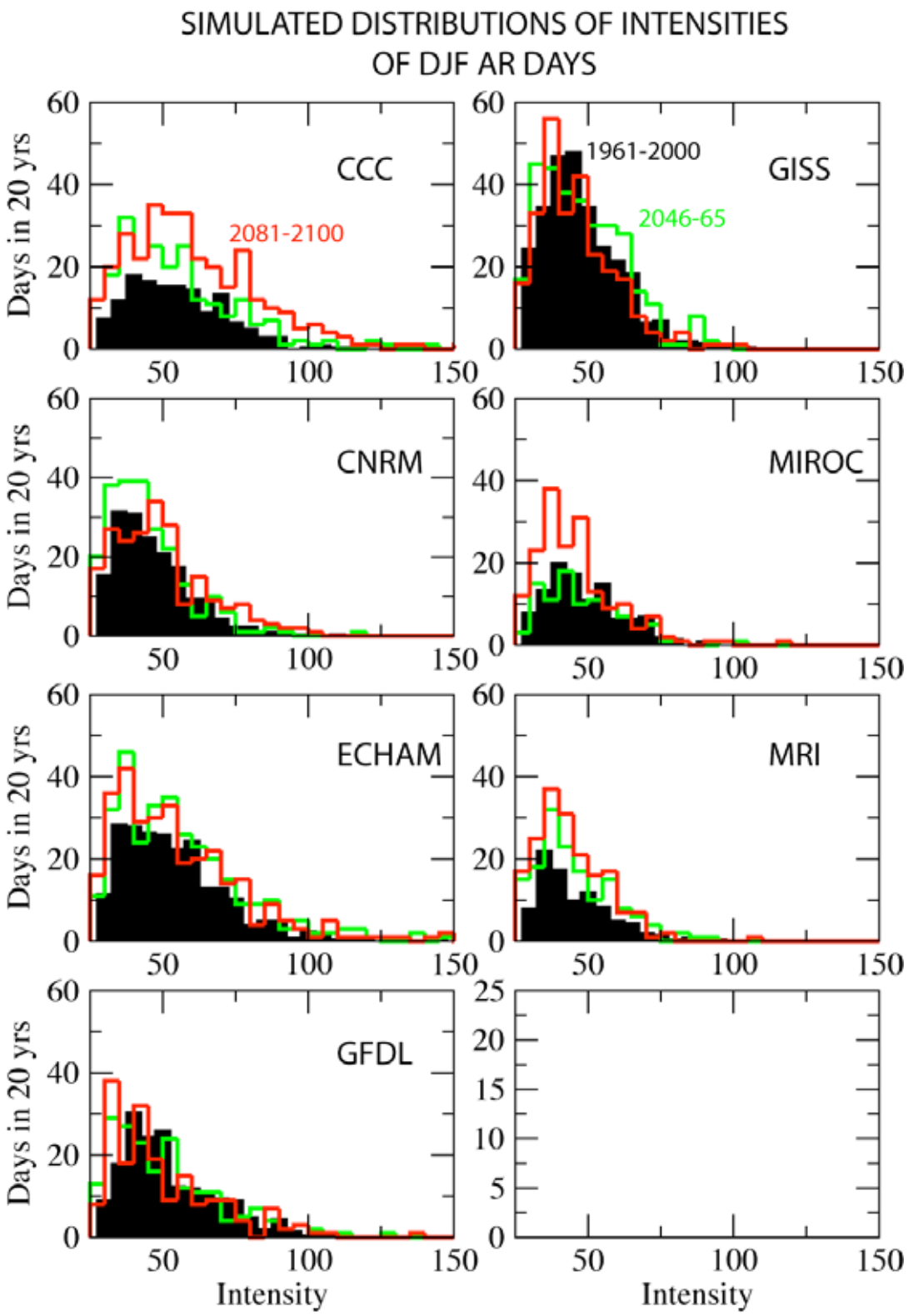

Figure 14. Same as Figure 12, except for intensities (IWV * upslope wind) on AR days

AR storms are associated with floods because of their relatively warm temperatures as well as the intense precipitation they can deliver. The warm temperatures associated with the ARs, because they draw upon air masses from far to the south over the subtropical and tropical Pacific Ocean, commonly result in elevated snowlines and thus much larger than normal river-basin areas receiving rain rather than snow. The rain runs off more quickly than snow, and floods can result. Thus it is important to also consider how temperatures on the simulated AR days evolve through the simulation periods.

The long-term AR-day and all-day averages of surface-air temperatures from the entire ensemble of projections are shown in Figure 15 for the 1961–2000, 2046–2065, and 2081–2100 epochs. In the historical simulations, AR-day temperatures average 1.8°C (3.2°F) warmer than the average of all December–February days, in close agreement with the Reanalysis average difference of 1.7°C (3.1°F). In the twenty-first century simulations, both AR-day average temperatures and all-day average temperatures increase, by about +1°C in 2046–2065, and by about +2°C (3.6°F) in 2081–2100. Notice that the AR-day average temperatures warm somewhat less quickly than all days as a whole, with all days warming by about 0.1°C more in 2046–2065 and by about 0.3°C (0.5°F) more by 2081–2100. This modest difference in the rates of average warming presumably reflects the fact that ARs involve transport of warm air from regions closer to the tropics, where overall rates of warming are less than in the midlatitudes (IPCC 2007). Roughly, the +1.8°C warmer AR storms by the end of the twenty-first century might be expected to lift snowlines by about 1.8°C * (1 km per +6.5°C [11.7°F] warming) or +330 m on average, thereby increasing the average basin areas that receive rain rather than snow in many mountain settings. The tendency for the difference between AR-day and all-day temperatures to decrease through the twenty-first century suggests that the AR-day snowlines (which historically might average about 330 m above the average snowline considering all winter days) might only average about 280 m above the snowline considering all winter days by end of century. This would mean that the areas over which an "average" AR storm might deposit rain on a previous snowpack might actually decline as the century progress, although the decline is likely to be small (perhaps 50 m of altitude).

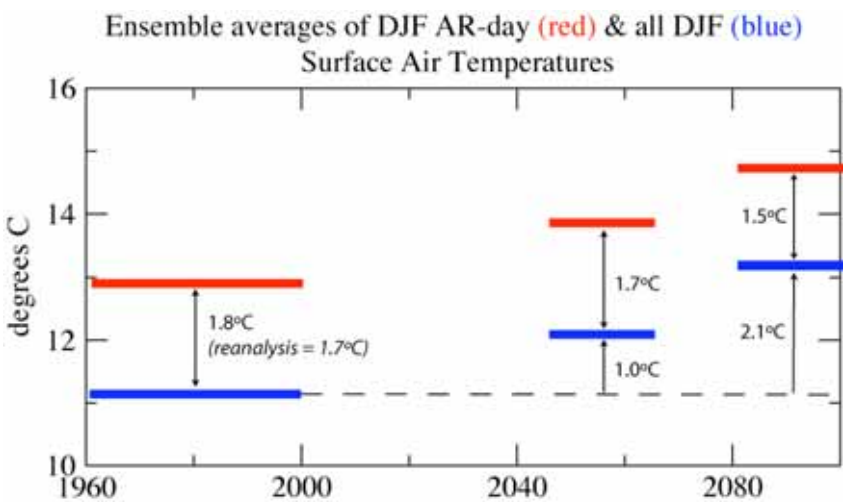

Figure 15. Ensemble average temperatures on December–February AR days (red) and on all December–February days (blue) under conditions corresponding to Figures 12–14

The full distributions of AR-day temperatures projected by each of the climate models are shown in Figure 16. Clearly the temperatures warm generally and, indeed, warm well beyond most of the historical range of natural variability in four of the seven models (CCC, CNRM, GFDL, and MIROC). These projected increases in the number of AR days with much warmer than (most) historical AR-day temperatures would ensure that, although the intensities of the upslope vapor transports may not increase dramatically, the basin areas receiving rain rather than snow is projected to increase dramatically in a significant number of AR storms in all of the models, and in most AR storms in four of the seven models. These increases in basin areas receiving rain are likely to result in large increases in the flood magnitudes from some AR storms, even as the number of AR storms also increases.

Finally, the seasonality of AR days was investigated by counting the numbers of such occasions for each month of the year in the historical, 2046–2065, and 2081–2100 periods (Figure 17). Generally speaking (with primary exception being the GFDL simulation), most of the increases in numbers of AR days under climate change occurred in the winter months, from about December to February. In five of the seven models, however, AR days also are projected to become notably more common in spring (CCC, GISS, MIROC, ECHAM and MRI) and autumn (CCC, GISS, and MRI). Thus, there is a widely simulated potential for the seasonality of dangerous AR storms to expand in response to climate change. This may imply more potential for increased early (pre-) and late (post-) historical flood-season flooding.

Thus the present analysis of AR storms off the central California coast in seven climate models predicts that (a) AR storms may arrive more frequently, with perhaps several more storms per winter, under the climate changes induced by A2 emissions, (b) the intensity of future AR storms may increase somewhat (but not by more than about 10% on average in the ensemble of projections considered here); and (c) the AR storms may warm by about 1.8°C, raising AR-storm snowlines by about 300 m on average, but that warming may not quite keep pace with overall winter warming so that the relations between AR snowlines and “normal” snowlines may change marginally. The rather pronounced increases in numbers of AR storms and in the temperatures of those storms suggest that the risks of major floods due to AR storms may increase both due to increased numbers of AR storms and due to increased rain-fed runoff during those storms. It is much less clear whether flood risks and conditions will change because of changes in the precipitation rates during those AR storms.

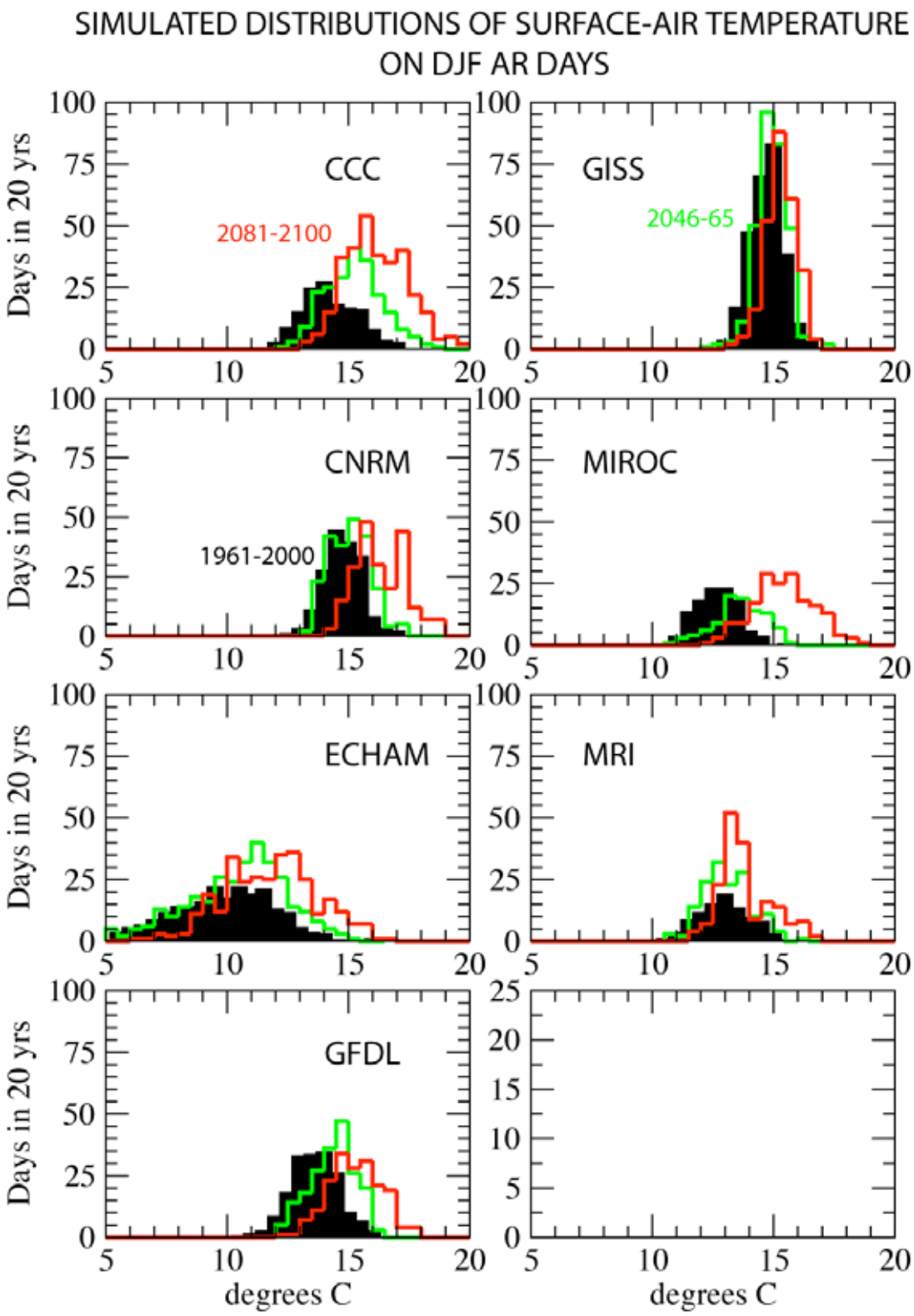

Figure 16. Same as Figure 12, except for surface-air temperatures on AR days

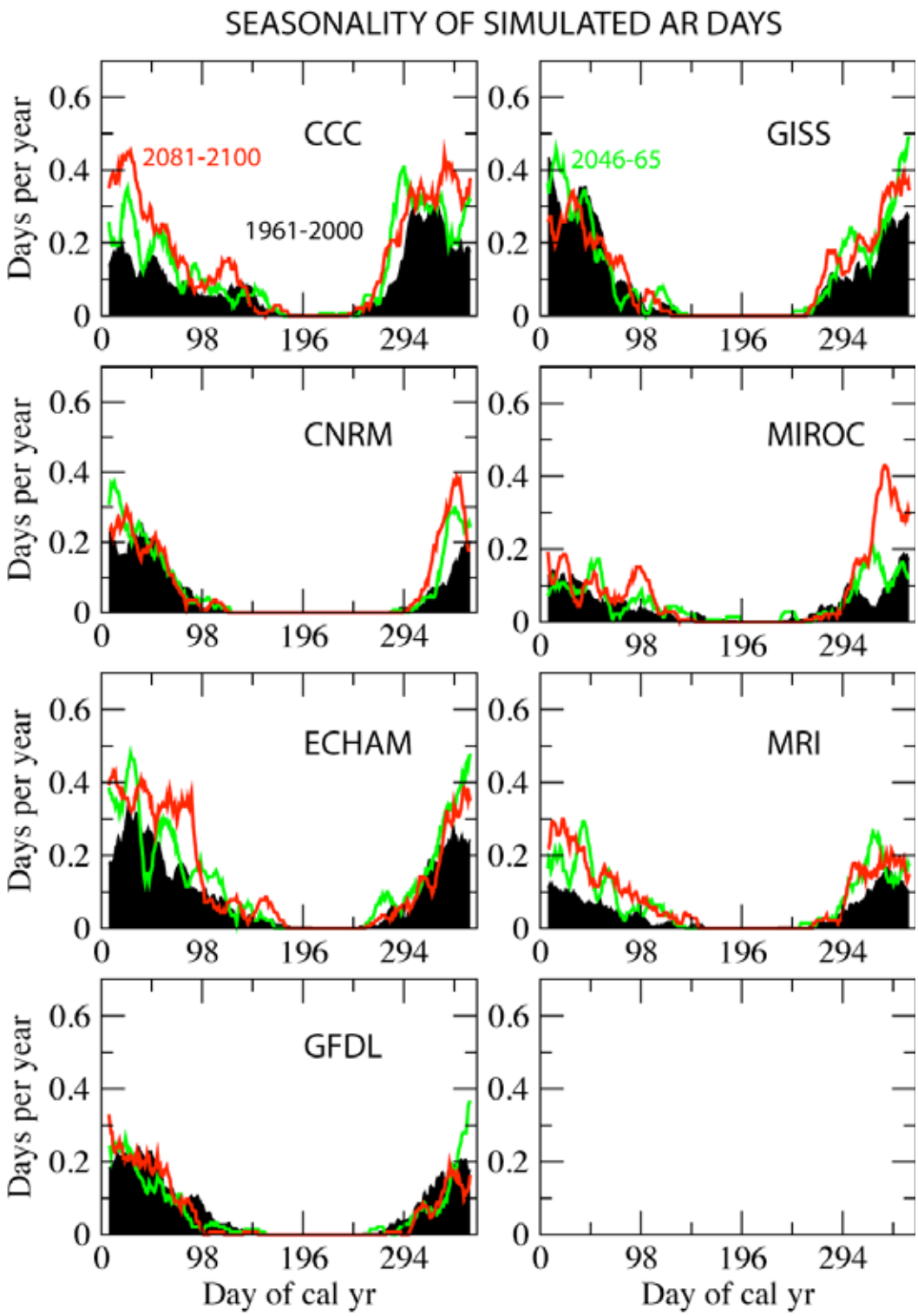

Figure 17. Simulated historical and projected (under A2 emissions) numbers of AR-days for each day of the calendar year; panels and coloring as in Figure 12. All curves have been smoothed with a 14-day moving average.

4.0 Hydrologic Simulation Analysis of Sierra Nevadan Floods

The occurrence of high-flow events or floods in simulated responses of daily Sierra Nevada streamflows to historical and projected-future climates were analyzed to evaluate the combined influences of climate variations, climate changes, and river-basin influences in the western Sierra Nevada. The simulated flood responses presented here are a natural bridge to other simulations of surface-water resource changes conducted as part of the state's overall climate-change assessment, which depends on the same hydrologic model and some of the same climate-change projections.

4.1. Method

Hydrological fluxes and conditions simulated by the VIC macroscale land-surface hydrological model—originally developed at the University of Washington and Princeton (Liang et al. 1994)—provide raw materials for analyses presented in this section. The VIC model has been used extensively in a variety of water resources applications; from studies of climate variability, forecasting and climate change studies (e.g., Wood et al. 1997, 2004; Hamlet et al. 1999; Nijssen et al. 1997, 2001). The model's soil moisture estimates are in reasonable agreement with the few point measurements available, while VIC-simulated streamflow validates well with observations when the model has been calibrated using river-discharge data, providing some confidence that VIC may usefully depict floods variability and change.

The VIC model was forced using observed meteorology (Hamlet and Lettenmaier 2005) and with downscaled GCM data, using the method of constructed analogues (CA) (Hidalgo et al. 2008). For a historical period, we analyzed VIC model-generated streamflows rather than monthly naturalized flows reported elsewhere, because VIC provides the daily streamflow needed for identifying individual flood events. For projections of future flood risks, climate simulations from three climate models were used: the CNRM CM3 model, the GFDL model, and the PCM model, all responding to the A2 emissions scenario (Figure 18).

The CA method is an analogous-based statistical downscaling approach described in detail in Hidalgo et al. (2008). The downscaled climate fields are obtained by constructing the downscaled patterns from linear combinations of previously observed weather patterns. The CA has skill in reproducing precipitation extreme events that is comparable to other statistical methods (Maurer and Hidalgo 2008).

The VIC-simulated runoff and baseflow were routed, as in Lohmann et al. (1996), to obtain daily streamflow rates for seven California rivers. The northern Sierra Nevada (NSN) total streamflow was estimated by adding the routed, daily streamflow values from the Sacramento River at Bend Bridge, the Yuba River at Smartville, and the Feather River at Oroville. The total streamflow from the southern Sierra Nevada (SSN) were obtained by adding together the routed streamflow values from four main tributaries of the San Joaquin River: the Stanislaus River at New Melones Dam, the Merced River at Lake McClure, the Tuolumne River at La Grange Dam, and the San Joaquin River at Millerton Lake. Flows surpassing the historical ninety-ninth streamflow percentile are designated here as floods.

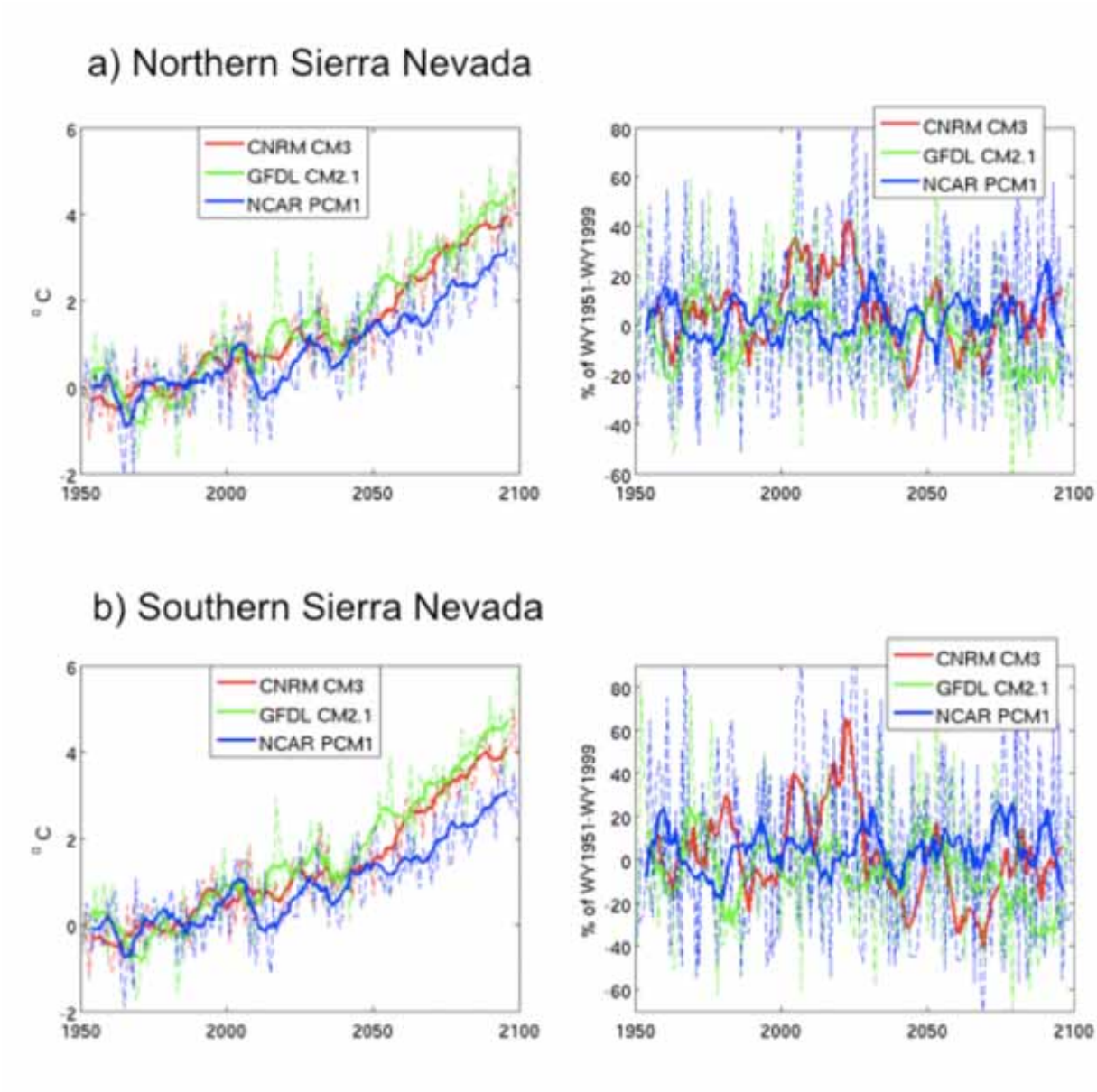

Figure 18. Ensembles of historical and future temperature and precipitation projections from three coupled ocean-atmosphere general circulation models, each forced by historical and 21st century A2 greenhouse gas emission scenarios; solid curves are seven-year moving averages, and dashed curves are annual deviations

Notably, because global-scale climate models operate on very coarse spatial grids (with grid cell centers separated by one to two degrees of latitude and longitude), the representation of topography and thus of orographic enhancements of precipitation, such as those associated with AR storms discussed previously, is almost entirely muted. As a consequence, the simulations reported in this section and the next section may not reflect the changes in AR-storm regimes reported earlier. Much more highly resolved climate simulations may be required to correct for this partial disconnect between the AR analyses and the hydrologic

simulations reported here and in the next section. Such resolutions are not yet available for the scenarios considered in this report.

4.2. Simulations of Changing Flood Risks

4.2.1. Northern Sierra Nevada

Historically, most of the floods in California's NSN have occurred from November to March (Figure 19a). As in the observations, the largest simulated floods have occurred during winter (DJF) and correspond to the so-called "pineapple express" events—discussed previously—in which strong low-level Pacific jets transport copious water vapor and warm temperatures to the West Coast (Figure 20; see also Cayan and Peterson 1989, 1993; Pandey et al. 1999; Cayan and Riddle 1992; Dettinger 2004; Mo et al. 2005; Ralph et al. 2006). During spring (MAM), smaller floods are common, and are associated with similar circulation patterns as the DJF floods but with lower intensity (not shown). In the simulations, there were already significant positive trends in the number of spring flood events in the NSN from 1950 to 1999 (not shown). Also, there has been an increasing trend in the frequency of extreme precipitation events (winter and spring) from 1950 to 1999 in the NSN (not shown), however this trend is not significant at the 95% confidence.

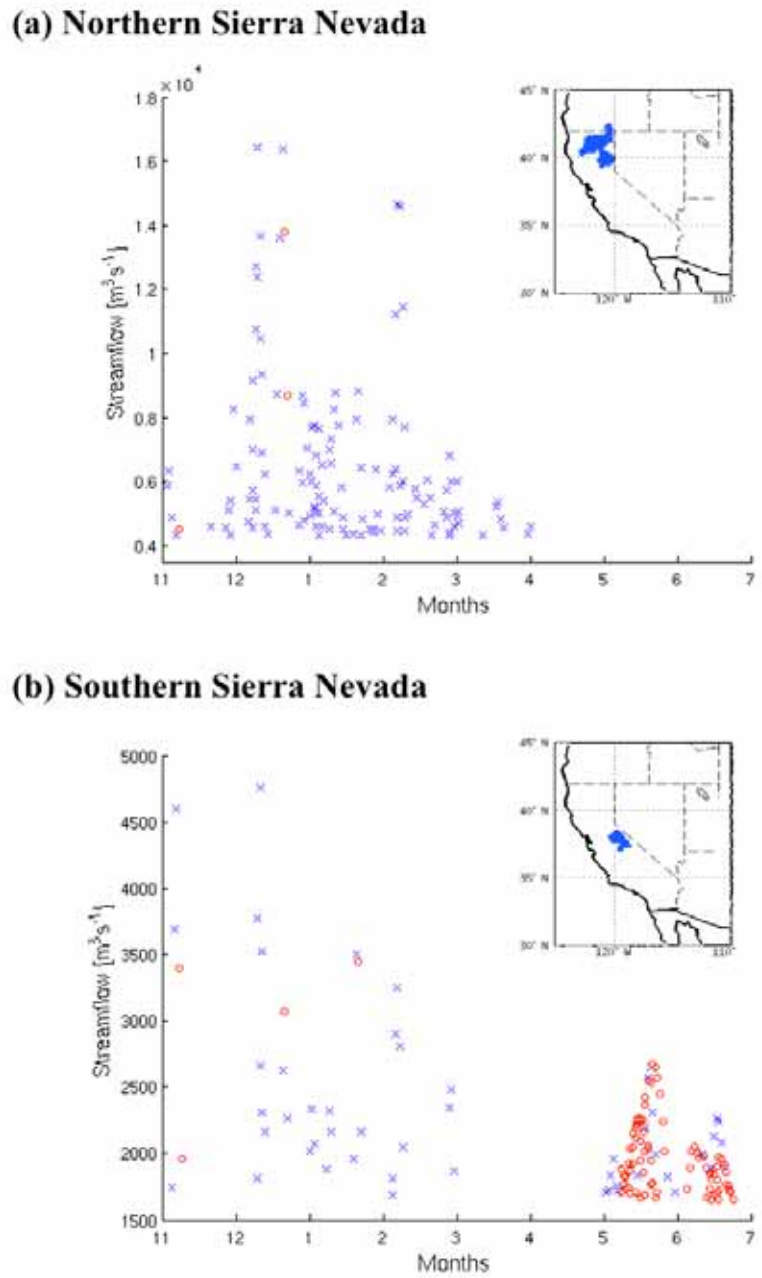

Figure 19. Floods in California's northern Sierra Nevada (a) and southern Sierra Nevada (b). In the figures, "X" symbols are precipitation-driven floods and red circle are snowmelt driven floods. Basin areas contributing to the floods are shown in inset maps.

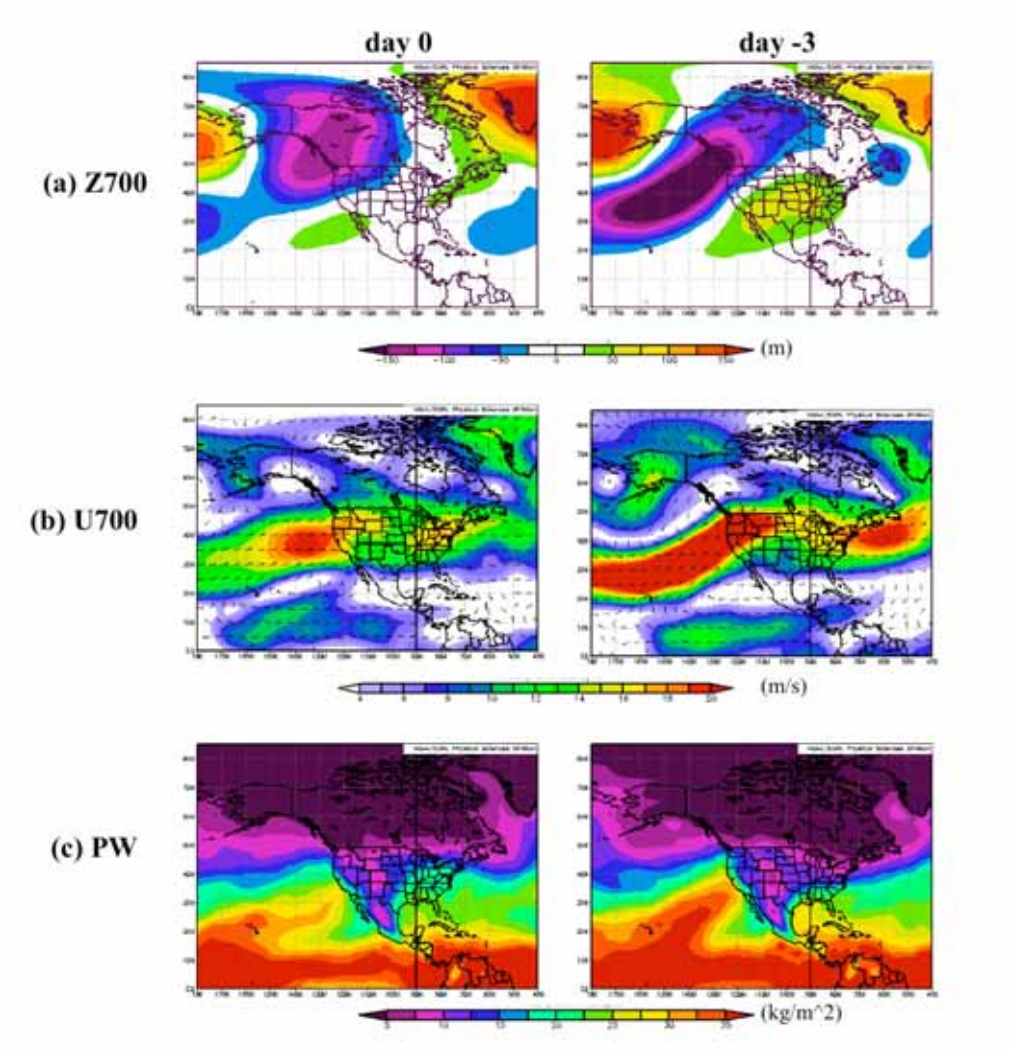

Figure 20. Composites of the 10 most extreme streamflow events occurring in Decembers–Februaries in the northern Sierra Nevada: (a) 700 mbar geopotential height anomalies (Z700); (b) 700 mbar mean wind speeds (U700); and (c) precipitable water (PW). In the panels, day 0 indicates the day of the flood events and day -3 indicated three days before the events. The panels were created using online compositing tools provided by NOAA's Climate Diagnostics Center.

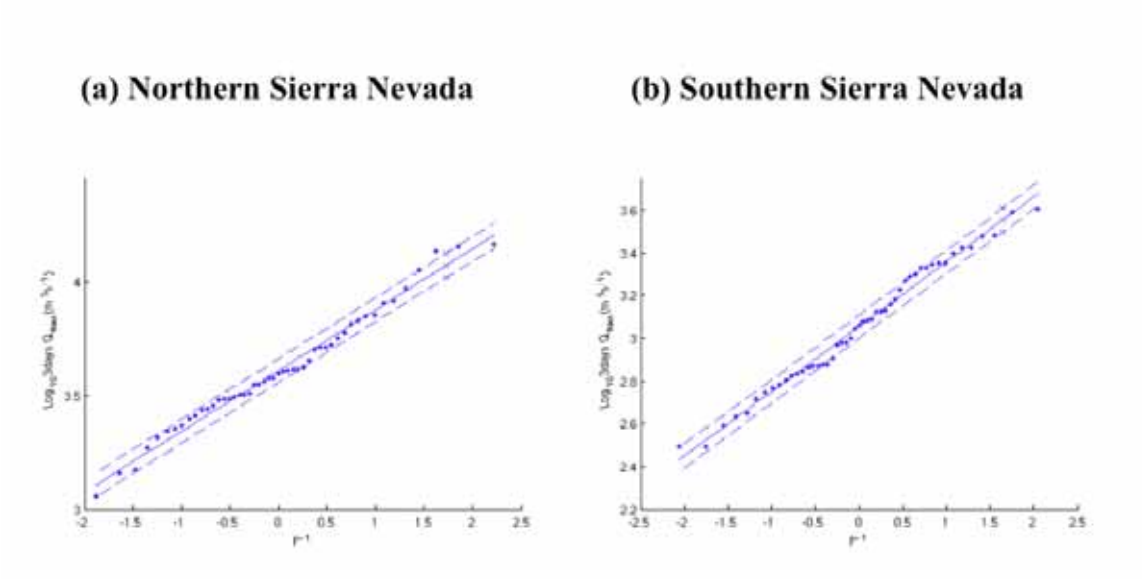

Figure 21. Frequency of the three-day annual maximum streamflows for the 1950–1999 period in the northern Sierra Nevada (a) and southern Sierra Nevada (b)

A flood frequency analysis of the historical three-day floods is shown in Figure 21. In this figure, the three-day maximum floods for each year were calculated along with their probabilities of exceedance (assigned using the Weibull plotting position). Then the inverse of the probability (P^{-1}) was calculated assuming a log-Pearson type III distribution.[3] The P^{-1} values were plotted against the base-10 logarithm of the three-day streamflow maximum. A least-squares linear regression was computed from the data along with 90% estimation confidence intervals. From these fits and confidence intervals, the hypothesis that the best prediction of streamflow for a certain return period T in years (Q_T) from the historical period was statistically different than the best prediction of Q_T under the altered (future) climate was tested by determining the simulations in which there was no overlap of the confidence intervals.

Sensitivity analyses of the flood frequency changes associated with prescribed changes in temperature (+3°C and +5°C) and precipitation (+10 %) showed increased magnitudes of the Q_{20} and higher floods, however the changes were not significant at the 90% confidence level (not shown). This suggests that it is difficult to change significantly the flood frequency curves of this basin.

The flood frequency analysis was also computed for the 20c3m (twentieth-century climate) from 1951 to 1999, for the climate change runs for an early period of the twenty-first century (2001 to 2049), and for a late period of the twenty-first century (2051–2099). Figures 22 and 23 show the intervals for the Q_{20} ("x" symbols), and Table 4 is a summary for different return periods. As can be seen, for the NSN there is a general increase in the Q_T in the future climate, but only in the case of the CNRM CM3 model for the late epoch (2051–2099) this change is significant at the 90% confidence for a variety of return periods (Table 4). In general, the frequency of floods

[3] The use of log-normal distribution instead of log-Pearson III does not change the results.

increases in the future for three models considered (Figures 23 to 26), and some of the projected floods have unprecedented large magnitudes when compared to the historical scenarios.

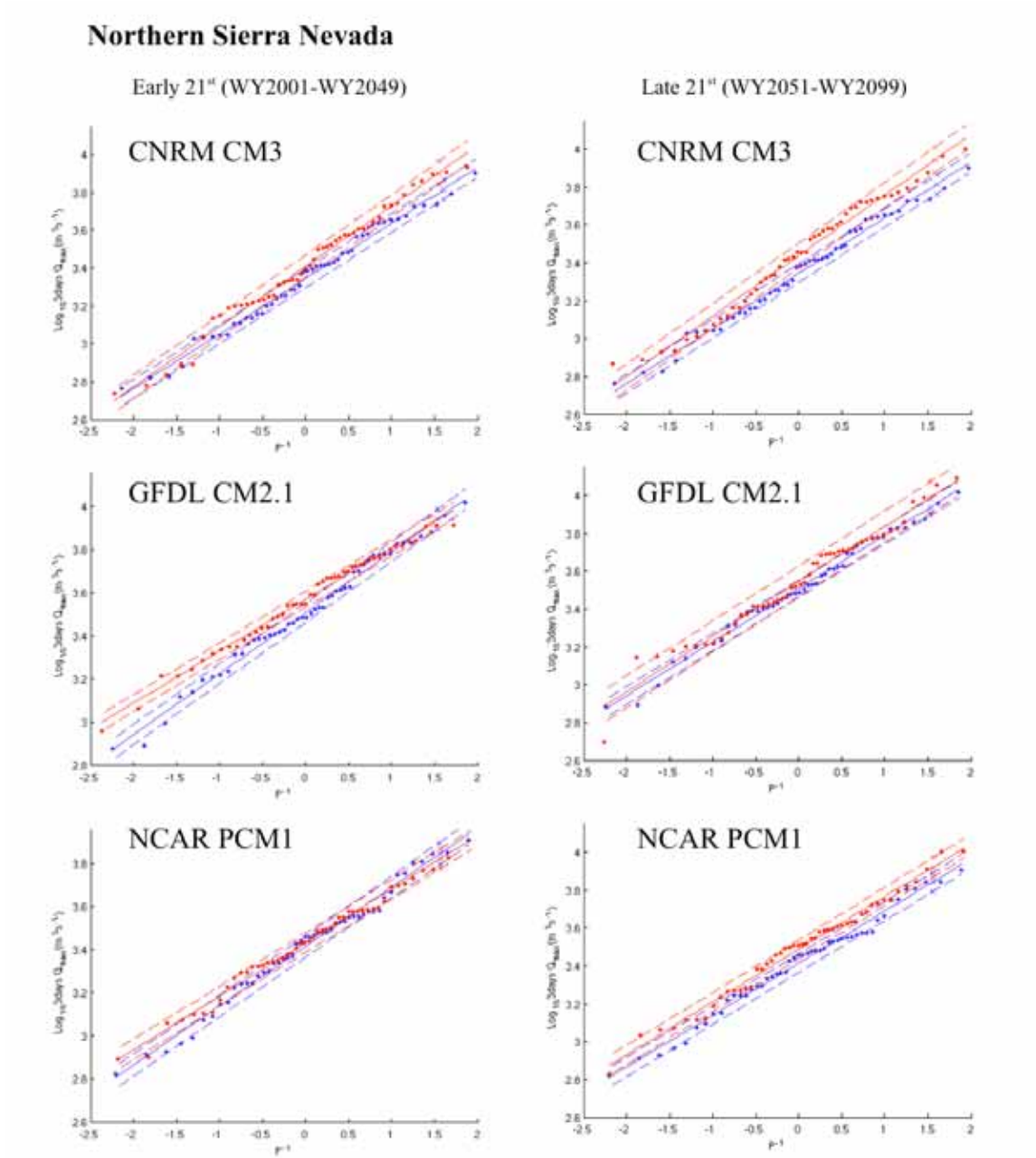

Figure 22. Frequency of the three-day annual maximum streamflows in the northern Sierra Nevada under climate change projections from three coupled ocean-atmosphere general circulation models, each forced by historical (blue curves) and 21st century greenhouse-gas A2 emission scenarios (red)

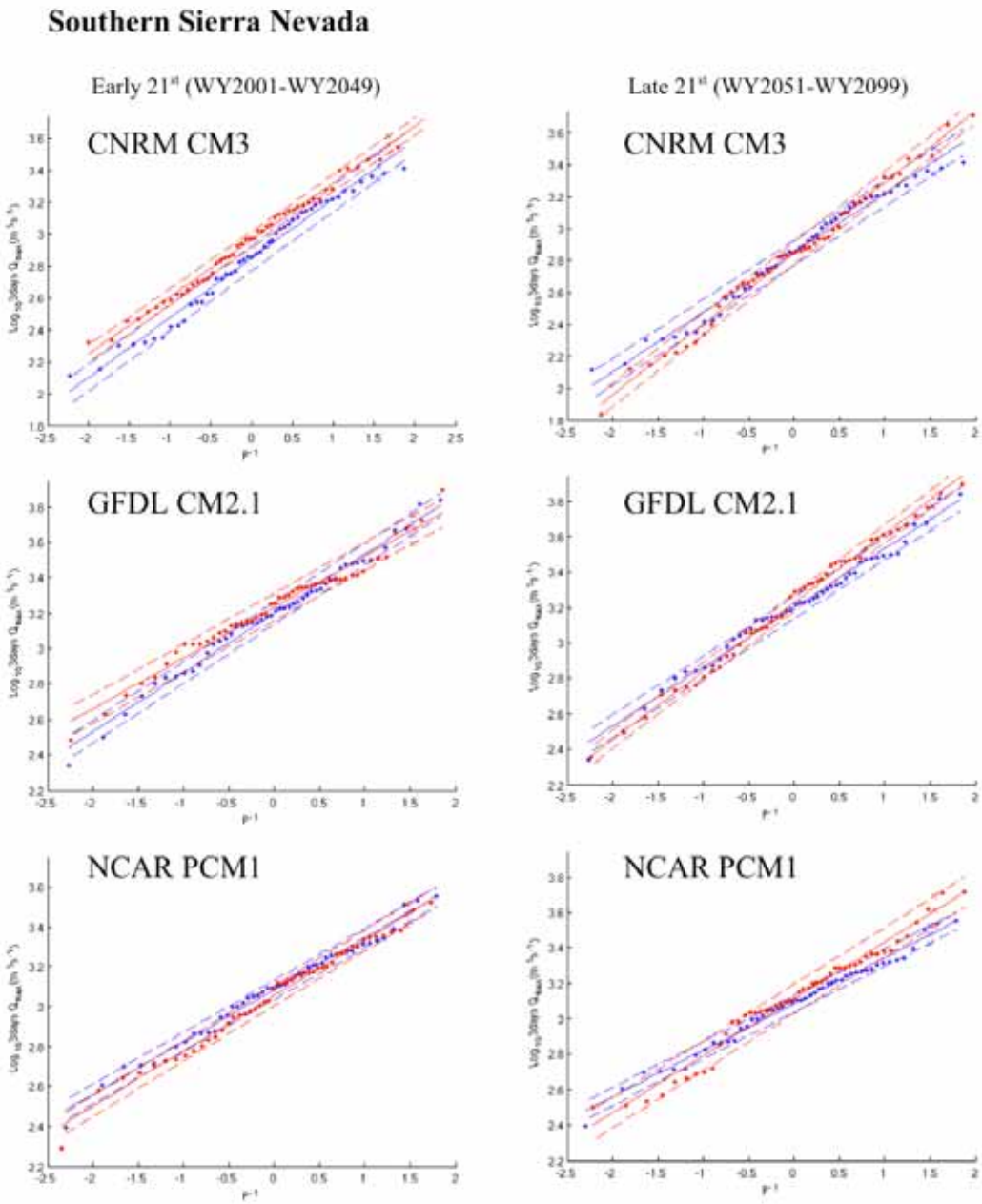

Figure 23. Same as Figure 22, except for the southern Sierra Nevada

Table 4. Three-day maximum floods from flood frequency analyses using log-Pearson III distributions; boldface where statistically different from floods in 1950–1999 period

Northern Sierra Nevada

T	Q_{20c3m}	Low Q_{20c3m}	High Q_{20c3m}	Q_{early}	Low Q_{early}	High Q_{early}	Q_{late}	Low Q_{late}	High Q_{late}
	(WY1951-1999)			(WY2001-WY2049)			(WY2051-WY2099)		
CNRM CM3									
2	2252	2011	2521	2669	2330	3057	2816	2419	3277
5	3924	3501	4398	4805	4190	5510	**5130**	**4402**	**5977**
10	5197	4632	5832	6399	5573	7347	**6920**	**5930**	**8076**
20	6524	5807	7329	8023	6978	9224	**8798**	**7527**	**10284**
50	8384	7450	9434	10234	8886	11787	**11441**	**9767**	**13400**
GFDL CM2.1									
2	3348	3019	3713	3915	3591	4268	3685	3058	4440
5	5607	5052	6222	5933	5438	6472	6243	5173	7534
10	7186	6469	7983	7162	6560	7818	8025	6639	9700
20	8728	7850	9705	8249	7551	9011	9754	8055	11810
50	10742	9649	11959	9531	8718	10421	11994	9885	14554
NCAR PCM1									
2	2680	2392	3003	2768	2497	3069	3163	2824	3542
5	4460	3977	5001	4390	3956	4872	5309	4736	5952
10	5724	5098	6426	5518	4967	6129	6854	6108	7691
20	6975	6206	7840	6622	5955	7363	8397	7475	9434
50	8637	7674	9722	8076	7253	8993	10468	9303	11778

Southern Sierra Nevada

T	Q_{20c3m}	Low Q_{20c3m}	High Q_{20c3m}	Q_{early}	Low Q_{early}	High Q_{early}	Q_{late}	Low Q_{late}	High Q_{late}
	(WY1951-1999)			(WY2001-WY2049)			(WY2051-WY2099)		
CNRM CM3									
2	741	616	892	907	806	1022	719	612	844
5	1470	1220	1771	1830	1624	2063	1669	1419	1962
10	2049	1698	2472	2664	2360	3007	2556	2170	3010
20	2659	2200	3215	**3649**	**3228**	**4125**	3610	3060	4259
50	3518	2904	4263	**5225**	**4612**	**5919**	**5284**	**4468**	**6249**
GFDL CM2.1									
2	1664	1443	1918	1785	1494	2132	1788	1593	2008
5	3048	2641	3518	3018	2523	3611	3626	3227	4076
10	4068	3520	4700	3889	3246	4659	5098	4532	5736
20	5092	4401	5891	4744	3953	5693	**6658**	**5911**	**7498**
50	6460	5574	7486	5866	4877	7055	**8854**	**7850**	**9986**
NCAR PCM1									
2	1273	1140	1422	1208	1075	1357	1351	1117	1635
5	2031	1817	2271	1961	1744	2205	2438	2012	2954
10	2529	2260	2830	2447	2174	2754	3251	2678	3946
20	2993	2672	3352	2892	2567	3258	**4079**	**3354**	**4960**
50	3571	3184	4004	3435	3046	3874	**5207**	**4272**	**6347**

4.2.2. Southern Sierra Nevada

There are two different kinds of floods in the SSN according to whether it rains or not during the days of the flood (Figure 19b). Thus there are "wet" or precipitation-dominated floods and "dry" or snowmelt-dominated floods (see also Roos 2006). As in the NSN the largest floods occur during the winter (DJF), corresponding to precipitation-dominated floods associated with the influence of the Pacific jet (not shown). Snowmelt-dominated floods occur mainly during the spring-summer (MJJ) and are associated with a high-pressure pattern located in the western United States that blocks the jet and brings higher than normal temperatures through subsidence (not shown). The DJF floods evolve quickly, while the MJJ floods present a more gradual increase of the flow. The DJF floods are observed two days after the precipitation, soil moisture and temperature peaks.

Sensitivity analyses of the flood frequency changes associated with prescribed changes in temperature and precipitation showed that the flood magnitudes for return periods greater or equal than 20 years would increase significantly in experiments in which the air temperature was increased by 5°C (9°F) and in the case where the snow production in VIC was turned off (not shown). The higher dependence of the SSN on snow (compared to the NSN) reflects the higher sensitivity to large warming and elimination of snowpacks prescribed in these severe experiments. Other less severe experiments in which the temperature was increased only by 3°C or precipitation was increased by 10% still showed increases in the magnitudes of the Q_{20} and higher floods, however the changes were not significant.

With respect to the climate projections, in general, there is an increase in the three-day flows for the future projected scenarios. However, these increases are not significant except for some of the cases. The Q_{50} significantly increases in all of the models during the 2051–2099 epoch. The Q_{20} also significantly increases in the GFDL CM2.1 and NCAR PCM1 during the 2051–2099 epoch. Also in the case of the CNRM CM3 the Q_{20} and Q_{50} significantly increase during the 2001–2049 epoch.

As in the NSN, in general the frequency of floods in the SSN stays the same or increases in the future (Figure 24, 25, and 26). Although there is no clear indication of a change in the seasonality of the floods, it is apparent that a few of the projected floods have unprecedented large magnitudes when compared to the historical scenarios.

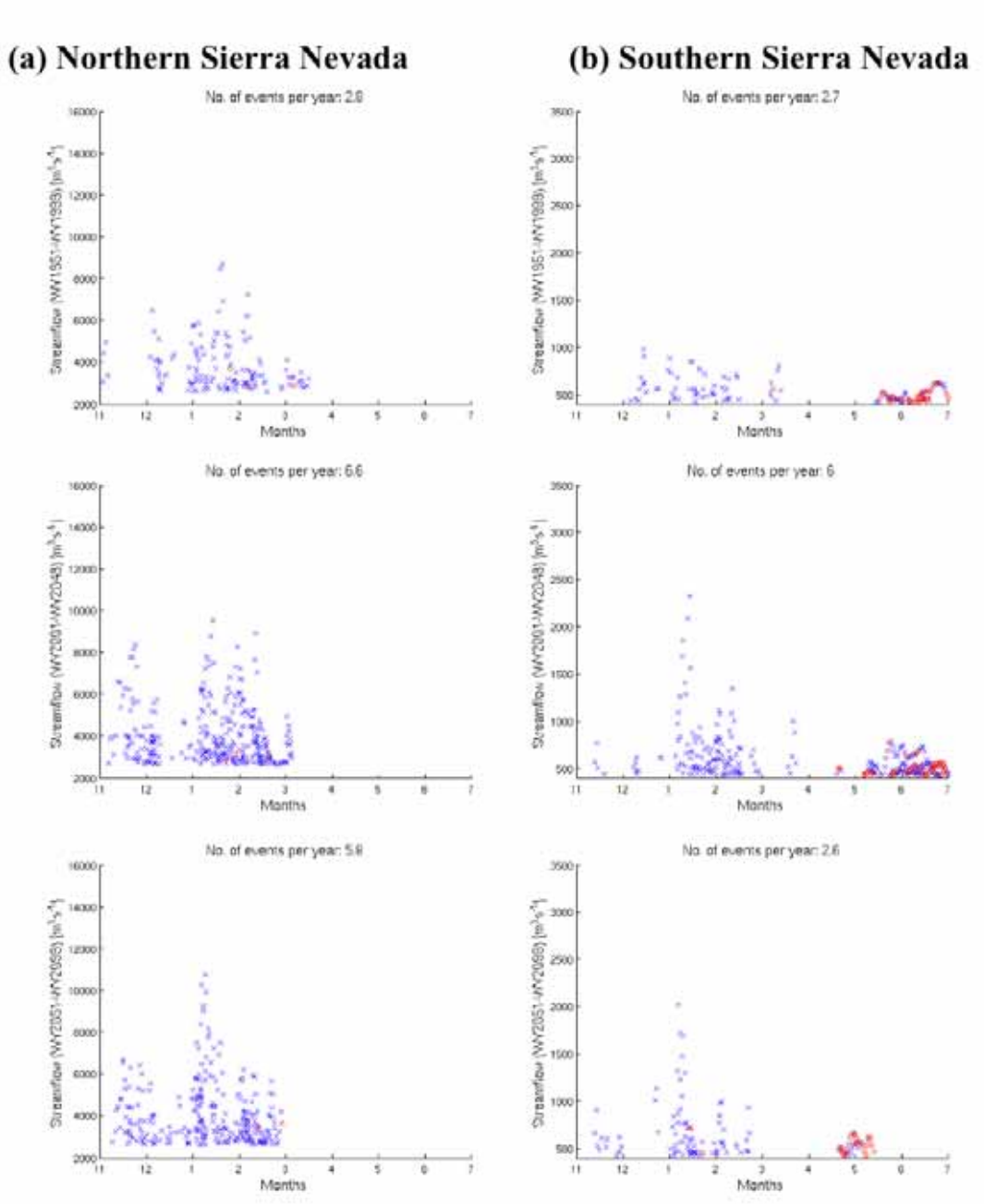

Figure 24. Floods in northern Sierra Nevada (a) and southern Sierra Nevada (b) in the 21st century, as simulated by the CNRM CM3 global climate models under 21st century A2 emissions scenario; "X" symbols are precipitation-driven floods and red circles are snowmelt driven floods

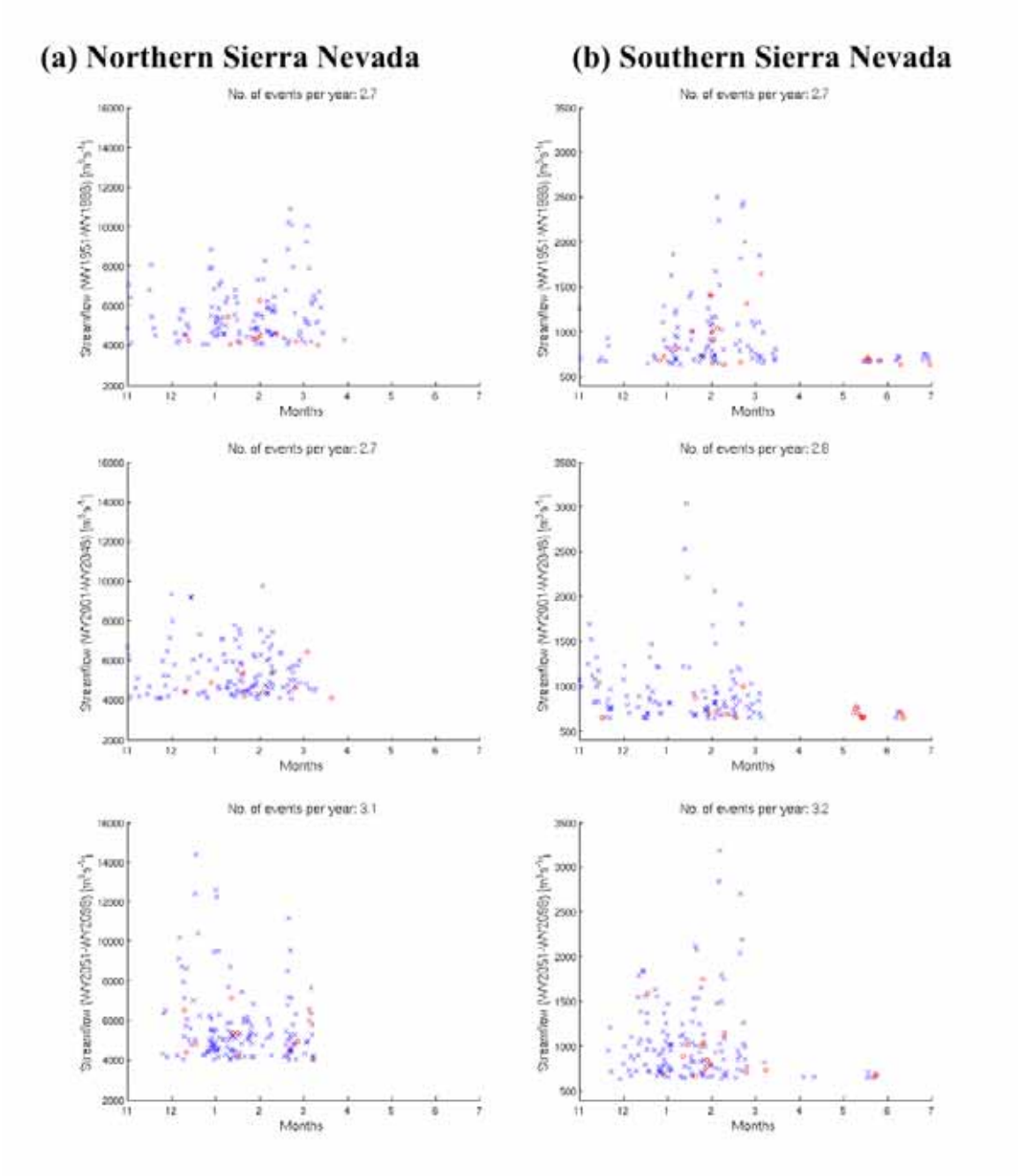

Figure 25. Same as Figure 24, except for simulation by the GFDL CM2.1 global climate model

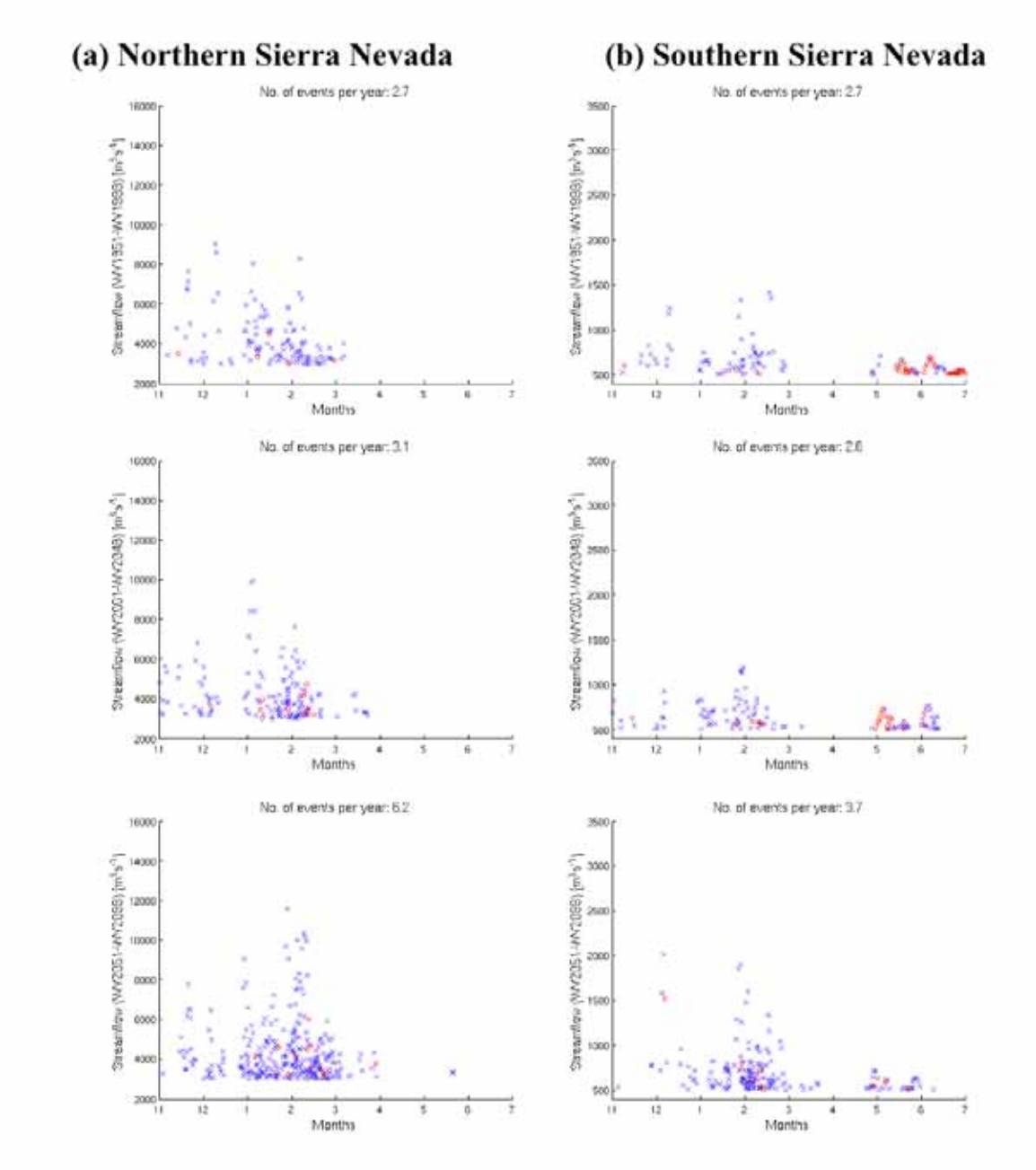

Figure 26. Same as Figure 24, except for simulation by the NCAR PCM global climate model

4.3. Summary

In the NSN and the SSN large floods have been observed historically during the winter (DJF). The DJF floods are associated with the influence of the Pacific jet, with the largest ones produced by relatively narrow surges of moisture from the tropics referred as atmospheric rivers.

There are also spring floods in the NSN that have similar characteristics as the DJF floods, but with lower intensity. In the SSN there are floods in MJJ that have different characteristics as the DJF floods. Specifically, the MJJ floods are snow-controlled and can be produced with no rain. These MJJ floods have the same order of magnitude as the DJF floods.

Severe warming has a stronger effect in the magnitude of three-day floods in the SSN than in NSN. The higher dependence of the SSN on snow (compared to the NSN) reflects the higher sensitivity to severe warming and elimination of snowpacks prescribed in the "$\Delta T=+5^{\circ}C$" and "no-snow" experiments. These experiments showed however that in order to change the flood frequency curves significantly it is necessary to introduce severe changes in the hydroclimatic conditions of the basin.

Analyses of future projections of flooding reveal that in the NSN there is a general tendency toward the increase in the magnitude of three-day flood events but this increase is statistically significant in only one of the three GCM models analyzed. In the case of the SSN, the magnitudes of three-day flood events increases also, but is significant only for the Q_{20} and Q_{50} floods in the second half of the twenty-first century. Also in both of the basins, a few of the projected floods have unprecedentedly large magnitudes when compared to the historical scenarios.

5.0 Tides, Storm Surges, and Floods

The impacts of increased magnitudes of floods of the sort discussed in the preceding section can be amplified in areas that lie near sea level by concurrent high sea level stands associated with astronomical tides, storm surges, El Niño influences, and the gradual sea-level rise that is projected to accompany global warming associated with increasing greenhouse-gas concentrations (Cayan et al. 2008c). In terms of largest scale threats in California, although they will be vulnerable to pressure from either high sea-level stands (Mount and Twiss 2005) or high freshwater flood levels (Florsheim and Dettinger 2005), the aging levees of the San Francisco Bay and Delta estuary are likely to be especially vulnerable to combined pressures when conditions arise in which water levels rise due to simultaneous occurrences of both high sea levels entering from the seaward side of the estuary and high flood stages from the inland side. Under climate change, such high water stands may increase due to increased flood frequencies and magnitudes, and increasing high sea-level stands and extremes (Cayan et al. 2008c).

In Cayan et al. (2008c), our capacity to quantify potential changes in the frequency or impact of concurrent high sea-level stands and high flood stages was limited by inability to directly link atmospheric and astronomical influences on sea levels (at daily or finer time scales) to the coinciding storm conditions that might yield flood flows. In Cayan et al. (2008c), therefore the problem was approached by counting the number of times that high sea level stands (projected by a model that predicts sea levels from astronomical tides, sea level pressures, and El Niño status) coincided with low barometric pressures typical of winter storms, all of which could be derived directly from global climate models without any downscaling. The temperature and precipitation downscaling tools available at the time did not, however, preserve linkages to the day to day fluctuations of sea level pressures and tides, and so a more direct linkage of floods and high seas could not be investigated.

For the present study, the new constructed analogues method for downscaling temperatures and precipitation (Hidalgo et al. 2008) provides downscaled fields that are synchronized with daily weather sequences in the original climate-model projections, so that hydrologic responses—including floods—can be simulated and synchronized with the barometric pressures and tides that yield storm surges and high sea-level stands. Therefore an example of the kinds of changes in frequency of concurrent high seas and high flood stages can be directly simulated and assessed. To accomplish this, tropical sea-surface temperatures, global mean air temperatures, local sea-level pressures, astronomical tide predictions, regional air temperatures and regional precipitation were extracted from a single projection of historical and future (A2) climate variations by the GFDL CM2.1 global climate model. The sea-surface temperatures were used to infer El Niño status of the Tropics. Tides, barometric influences and El Niño status were used to project corresponding non-trending sea level variations at San Francisco. Global mean temperatures were used to estimate global sea-level rise, following the methodology of Rahmsdoff (2007), but with inclusion of the historical effects of water held in reservoirs (Chao et al. 2008). The resulting sea-level trends amount to a 1.09 m rise by 2100, and were added to the shorter term sea-level fluctuations at San Francisco to form a scenario of hourly sea levels from 1950 to 2100.

Daily regional air temperature and precipitation were downscaled by constructed analogues and used to simulate runoff generation with the Bay-Delta Watershed Model (BDWM) (Knowles and Cayan 2002). The BDWM is a physically based, soil moisture accounting model with a daily time step and horizontal resolution of 4 km over the entire Central Valley-Coastal Ranges-Sierra Nevada watershed draining to the San Francisco Bay-Delta estuary. The snow component of the model is an adaptation of the Utah Energy Balance snow model (Tarboton and Luce 1996), which faithfully reproduces Sierra Nevada snow variability. The BDWM has been used in several previous studies to project hydrologic responses to climate variability and change in the Bay-Delta watershed (e.g., Knowles 2002; Knowles and Cayan 2002, 2004). From the resulting hydrologic simulation, 1950–2100, runoff generated in the highland catchments of the Sacramento and San Joaquin basins, above the major foothill reservoirs in these basins, was accumulated to represent daily inflows to those reservoirs and indications of the timing and general magnitude of flood events in the catchments that drain toward the estuary. For the present study, those runoff totals were not routed through water-management models. The resulting simulated streamflows (Figure 27) include a few unprecedentedly large floods in the twenty-first century in the Sacramento River and a general enhancement of the normal-year peak flows in both rivers.

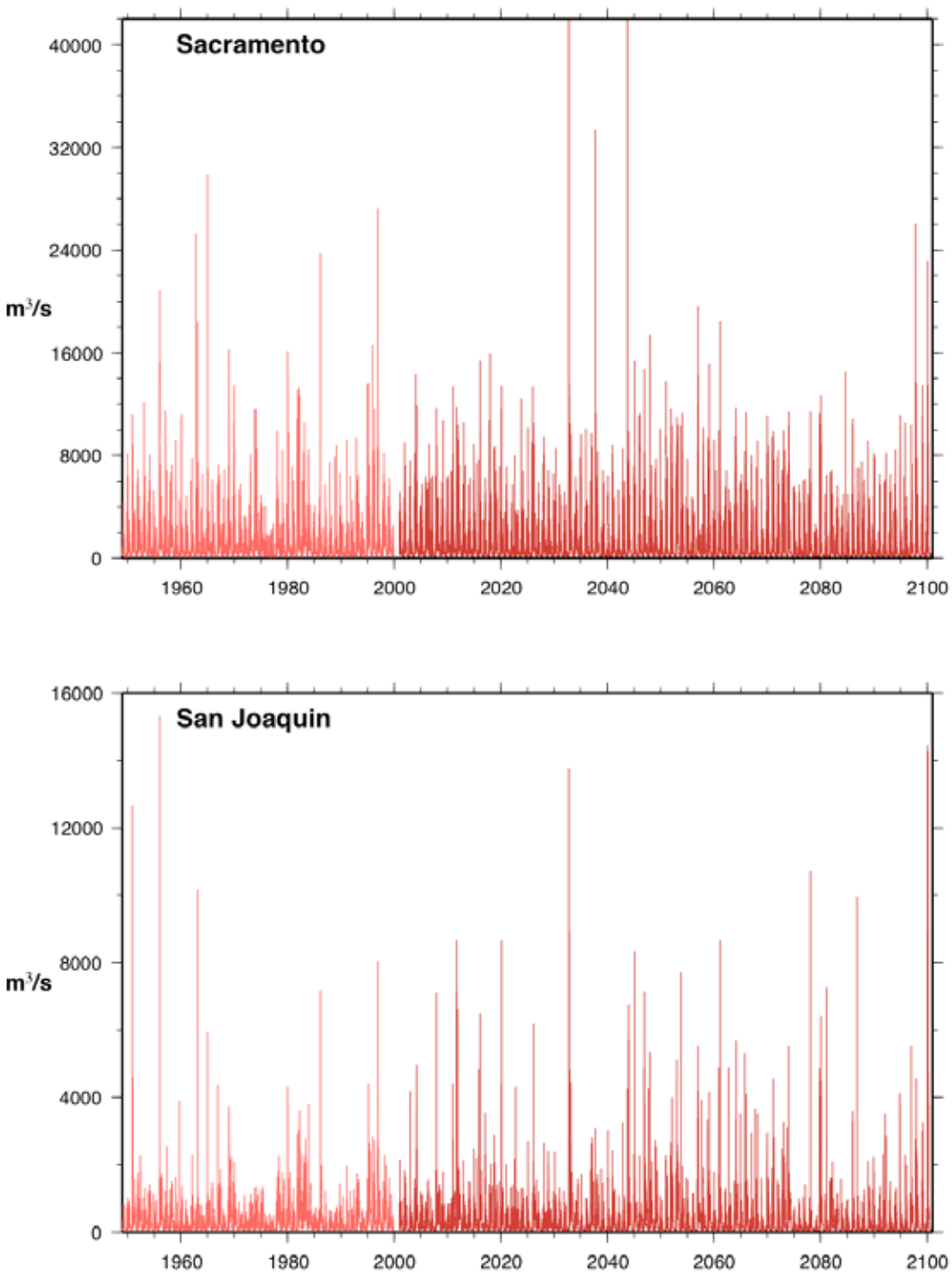

Figure 27. Simulated reservoir inflows in the Sacramento and San Joaquin River basins, from the Bay-Delta Watershed Model (Knowles and Cayan 2002) driven by simulated historical (20c3m) and future (A2 greenhouse-gas emissions) climates from the GFDL global climate model, downscaled by the constructed analogues method (Hidalgo et al. 2008)

Finally the projected sea levels were evaluated, and all instances when the sea level at San Francisco exceeded the 99.9% exceedance level (1.20 m above mean historical sea level) in the 1950–2005 period were noted. The combined Sacramento and San Joaquin reservoir inflows on each of the indicated days are plotted in Figure 28. Very often the high sea-level stands occur when river flows are small to moderate; however, on a disconcerting number of occasions, high sea-level stands coincide with high river flows. The number of occasions when high sea levels and high river flows coincide increase markedly in the twenty-first century under the GFDL A2 climate. For example, during the 1950–2000 period, flows on only two occasions of high sea-level stands reach 15000 m^3/s, whereas during the twenty-first century flows during high sea-level stands surpass that discharge more than 40 times. The flows during high sea level stands exceed 15000 m^3/s to a considerable extent on most of those high sea level/high flows occasions, rising to 30000 m^3/s on one occasion.

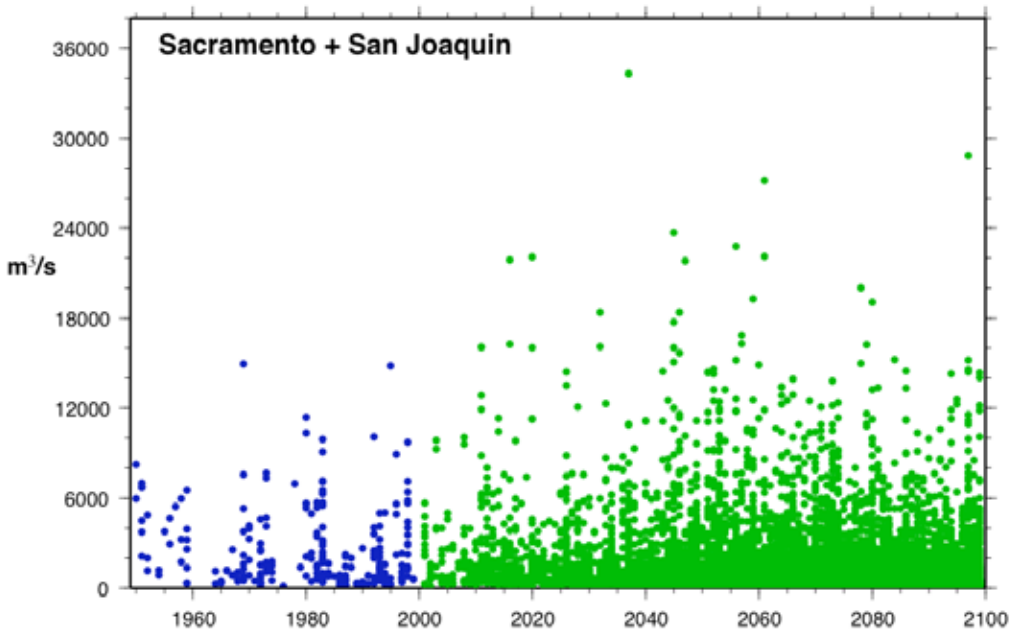

Figure 28. Simulated freshwater reservoir inflows in the Sacramento and San Joaquin River basins during days when projected sea levels are at or above the 1950–2005 99.9% exceedance level at San Francisco, under climatic conditions projected by the GFDL CM2.1 global climate model under historical and A2 greenhouse-gas emissions scenarios. Streamflows shown here are from the simulation displayed in Figure 27.

Thus the general drift toward moderately larger and more frequent floods simulated as following from the GFDL climate changes under A2 emissions combines with the relatively rapid sea-level rise projected under that scenario to yield many more occasions when high sea-level stands might combine with high flows and freshwater stages in the rivers to severely stress the levees of the Bay and Delta. The present study does not attempt to route the reservoir inflows through the flood-management operations at the state's reservoirs, and thus many of the flows shown in Figure 28 might be considerably ameliorated by reservoir operations in the

real world. Historically, though, reservoir management has not done as much to ameliorate the number of levee breaks in California as might be expected (Florsheim and Dettinger 2007). Thus, even the moderate sea-level rises and relatively modest flood frequencies increases currently being projected may be sufficient to threaten the estuary's levee systems as a result of more frequently coinciding flood stages.

More generally, combined impacts of sea level rise (and high sea-level stands) with concurrent flood flows have the potential to imperil many smaller coastal and estuarine settings and communities along the California coast. The remarkable increases shown in Figure 28 suggest that potential growth of these risks should be addressed more widely in future studies.

6.0 Conclusions

Major floods are a recurring theme in California's climatology and hydrology, with a long history of associated deaths and destruction. Historically, the most widespread and devastating floods in California have been associated with some of the largest, and generally warmest, winter storms, with massive runoff volumes from the Sierra Nevada and Coastal Ranges. Although uncertainties abound, the challenges of flood control may become more commonplace and extreme as a result of projected climate changes over California in the twenty-first century. Among the uncertainties that need to be narrowed in order to plan for future flood management are whether floods will be larger or smaller under climate change, more common or less common, and whether the seasonality of floods is likely to change. Several different analyses of potential changes in California's flood regimes were performed for this study, using a variety of data sets and models to address several potential flood-inducing processes.

From these analyses, we conclude—at least tentatively—that, with continued warming in the twenty-first century, certain changes in California's flood regimes seem likely: Higher snowlines will probably increase the frequency of flooding due to more frequent occasions of large-scale rainfall runoff. Some of the additional floods may be larger than historical floods due to opening of even larger-than-historical areas of river basins to receive rainfall rather than snow—especially in the higher southern parts of the Sierra Nevada. Chances for floods may be incremented due to wetter winter soils resulting from warming-induced "winter drizzles" of intermittent snowmelt into highland soils. Opportunities for coincidence of high sea level stands with high flood stages in the lowlands may also increase as flood frequencies increase and sea levels rise.

Other changes are more difficult to project, and simulation models were used here to try to weigh the competing influences that might either increase or diminish future floods. Overall, both the VIC and BDWM hydrologic models responded to downscaled climate-change projections with increases in flood frequencies and magnitudes, but neither yielded large changes in that regard. The southern Sierra Nevada, according to the models, may be at greater risk of increased flooding because they have so much more area that has historically received mostly snowfall and not contributed much to flooding, but which has the potential to transition into flood contributors in a wetter world.

The twenty-first century incidence and characteristics of major winter storms, in particular pineapple express or atmospheric river storms, were assessed here in the context of climate

changes projected in an ensemble of seven different climate models under the rapid greenhouse-gas emissions of an A2 scenario. Projected changes in these storms are most common at the extremes: Years with many AR storms become more frequent in most climate change projections analyzed here, but the average number of such storms per year are not projected to change much. Likewise, although the average intensity of these storms is not projected to increase much in most models, occasional much-larger-than-historical-range storm intensities are projected to occur under the warming scenarios. The seasonality of such storms is projected to expand in most of the climate models, resulting in increased chances of pre- and post-season storms and flooding, where "pre-" and "post-" refer to the historically typical December–March flood seasons in California. Finally the AR storms warm along with, but not quite as fast as, the general mean temperatures in the seven projections analyzed.

This paper is not intended to provide final, quantitative projections of flood-frequency changes in California under twenty-first century climate change. More research is needed prior to making such detailed judgments and projections. The present study has focused on and evaluated various physically based approaches to understanding future flood regimes, and much additional research will be necessary to strengthen and focus these results. Both the changes listed above as being likely to happen and those that are difficult to project will require more attention. In particular, because of the strong influences that the topographies of individual basins and subbasins on flood characteristics, more site- and river-specific research will be needed if reliable, quantitative estimates of future flood statistics for engineering and planning uses are to be developed. It will be necessary to achieve a much better understanding of the geographic distributions of changes in storm characteristics and frequencies than the single-trajectory analysis demonstrated here, because southern and extreme northern parts of the state may experience much different changes in atmospheric-river storm statistics than the central California case evaluated here. Within storms, more detailed research is needed to infer likely future changes and ranges of snowline variations, precipitation maxima and intensities, atmospheric-stability conditions, and warm-cool storm sequencing. Two land-surface hydrologic models were used here to simulate flood changes and gave broadly similar results, but a much better understanding is needed of the necessary model characteristics and experimental designs for simulating realistic flood-frequency changes. To date, watershed models used for such evaluations (here and in the literature) have been models that were calibrated with more attention placed upon longer term flow variations, like timing of peak flows and monthly to annual flow totals, than upon details of relatively infrequent flood extremes.

All of these physically based research topics would best be pursued in parallel with research to extend traditional statistically based flood-frequency evaluations for use under changing climate conditions. Statistical methods can provide much-needed ground truth to more model-based approaches but face the difficult problem of continual reevaluations of methods and data resources as the climate changes. Traditional statistical approaches assume that observed flood histories are random samplings from some ideal, unchanging, underlying probability distributions. Under climate change, the underlying distribution of floods will likely change (as discussed throughout this report) and the methods will need to be modified to account for these changes under continuing uncertainties as to what the changes will be. Some data may be better suited to making future-flood frequency estimates, e.g., the most recent data may become increasingly more informative than data from the distant, historical past, but where to draw the

line between applicable and non-applicable data will be a difficult puzzle in the real world. Methods that retain as much data as possible while weighting the most relevant data more than the less relevant data will need to be developed and applied. Safe margins of error for flood-control and management designs will need to be developed using much the same data resources. In each case, because past observations are unlikely to be reliable indicators of future flood statistics, these statistical methods will need to be informed and tested on results from the physically based approaches, and vice versa.

Thus, while we can begin already to infer the directions and even some broad magnitudes of future changes in California's flood regimes using tools already at hand, large uncertainties remain. New methods and analyses will likely need to be developed to provide quantitative guidance for detailed planning of flood management and integration of flood-control with water-supply management under future climate change.

7.0 References

Andrews, E. D., R. C. Antweiler, P. J. Neiman, and F. M. Ralph. 2004. "Influence of ENSO on flood frequency along the California coast." *J. Climate* 17:337–348.

Bao, J.-W., S. A. Michelson, P. J. Neiman, F. M. Ralph, and J. M. Wilczak. 2006. "Interpretation of enhanced integrated water-vapor bands associated with extratropical cyclones: Their formation and connection to tropical moisture." *Mon. Wea. Rev.* 134:1063–1080.

California Department of Water Resources (DWR). 2005. *The California water plan update 2005—Highlights.* DWR Bulletin 160-05. www.waterplan.water.ca.gov/docs/cwpu2005/cwphighlights/highlights.pdf.

California Department of Water Resources (DWR). 2009. The California water plan update 2009: Pre-administrative draft, DWR Bulletin 160-09, Chapter 7—Implementation Plan. www.waterplan.water.ca.gov/cwpu2009/vol1/index.cfm.

Cayan, D. R., and D. H. Peterson. 1989. "The influence of North Pacific atmospheric circulation on streamflow in the West." AGU Monograph 55, *American Geophysical Union* 375–397.

Cayan, D. R., and D. H. Peterson. 1993. "Spring climate and salinity in the San Francisco Bay Estuary." *Water Resources Research* 2:293–303.

Cayan, D. R., and L. Riddle. 1992. Atmospheric circulation and precipitation in the Sierra Nevada: Proceedings, International Symposium on Managing Water Resources During Global Change. American Water Resources Association, Reno, Nevada, Nov 1–5.

Cayan, D. R., E. P. Maurer, M. D. Dettinger, M. Tyree, and K. Hayhoe. 2008a. "Climate change scenarios for the California region." *Climatic Change* 87(Suppl 1), doi10.1007/s10584-007-9377-6, S21–S42.

Cayan, D., M. Tyree, M. Dettinger, H. Hidalgo, T. Das, E. Maurer, P. Bromirski, N. Graham, and R. Flick. 2008b. Climate change scenarios and sea level rise estimates for the California 2008 Climate Change Scenarios Assessment.

Cayan, D. R., P. Bromirski, K. Hayhoe, M. Tyree, M. Dettinger, and R. Flick. 2008c. "Climate change and the potential for sea-level extremes along the California coast: Climatic Change." 87 (Suppl 1), doi10.1007/s10584-007-9376-7, S57–S73.

Chao, B. F., Y. H. Wu, and Y. S. Li. 2008. "Impact of artificial reservoir water impoundment on global sea level." *Science* 320:212, doi:10.1126/science.1154580.

Delta Vision Blue Ribbon Task Force. 2008. *Our vision for the California Delta.* Report to Governor Schwatzenegger. January 2008.

Dettinger, M. D. 2004. *Fifty-two years of pineapple-express storms across the West Coast of North America.* California Energy Commission PIER Energy-Related Environmental Research Report CEC-500-2005-004. 15 p.

Dettinger, M. D. 2005. "From climate-change spaghetti to climate-change distributions for 21st Century California." *San Francisco Estuary and Watershed Science* 3(1), http://repositories.cdlib.org/jmie/sfews/vol3/iss1/art4.

Dettinger, M., K. Redmond, and D. Cayan. 2004. "Winter orographic precipitation ratios in the Sierra Nevada—Large-scale atmospheric circulations and hydrologic consequences." *J. Hydrometeor.* 5:1102–1116.

Florsheim, J., and M. Dettinger. 2005. "Influence of anthropogenic alterations on geomorphic response to climate variations and change in San Francisco Bay-Delta and watershed." *Watershed Management Council Networker* 13(Spring 2005): 13–16.

Florsheim, J. L., and M. Dettinger. 2007. "Climate and floods still govern California levee breaks." *Geophysical Research Letters* 34(L22403), doi:10.1029/2007GL031702, 5 p.

Hamlet, A. F., and D. P. Lettenmaier. 1999. Effects of Climate Change on Hydrology and Water Resources in the Columbia River Basin. *Am. Water Res. Assoc.* 35(6): 1597–1623.

Hamlet, A. F., and D. P. Lettenmaier. 2005. "Production of temporally consistent gridded precipitation and temperature fields for the continental U.S." *J. of Hydrometeorology* 6:330–336.

Hidalgo, H. G., M. D. Dettinger, and D. R. Cayan. 2008. *Downscaling with Constructed Analogues: Daily Precipitation and Temperature Fields Over the United States.* California Energy Commission, PIER Energy-Related Environmental Research. CEC-500-2007-123. 48 pp. Available on-line: www.energy.ca.gov/2007publications/CEC-500-2007-123/CEC-500-2007-123.PDF

Intergovernmental Panel on Climate Change (IPCC). 2007. *Climate change 2007: The physical science basis. Summary for Policymakers.* IPCC Secretariat. www.ipcc.ch. 18 p.

Jain, S., U. Lall, and M. E. Mann. 1999. "Seasonality and interannual variations of Northern Hemisphere temperature: Equator-to-pole gradient and ocean–land contrast." *Journal of Climate* 12:1086–1100.

Jeton, A. E. 2006. Flood chronology of the Carson River basin, California and Nevada website. U.S. Geological Survey Fact Sheet 2006-3102, 2 p.

Kalnay, E., et al. 1996. "The NCEP / NCAR 40-Year Reanalysis Project." *Bull. Amer. Meteor. Soc.* 77:437–471.

Kelley, R. 1998. *Battling the inland sea—Floods, public policy, and the Sacramento Valley*. University of California Press. 420 p.

Knowles, N. 2002. "Natural and human influences on Freshwater Inflows and Salinity in the San Francisco Estuary at Monthly to Interannual Scales." *Water Resour. Res.* 38:25–1 to 25–11.

Knowles, N., and D. R. Cayan. 2002. "Potential effect of global warming on the Sacramento / San Joaquin watershed and the San Francisco estuary." *Geophysical Research Letter* 29:38-1 to 38-4, doi:10.1029 / 2001GL014339.

Knowles, N., and D. R. Cayan. 2004. "Elevational dependence of projected hydrologic changes in the San Francisco estuary and watershed." *Climate Change* 62:319–336.

Knowles, N., M. Dettinger, and D. Cayan. 2006. "Trends in snowfall versus rainfall for the Western United States." *Journal of Climate* 19(18): 4545–4559.

Liang, X., D. P. Lettenmaier, E. F. Wood, and S. J. Burges. 1994. "A Simple hydrologically Based Model of Land Surface Water and Energy Fluxes for GSMs." *J. Geophys. Res.* 99(D7): 14,415–14,428.

Lohmann, D., R. Nolte-Holube, and E. Raschke. 1996. "A large scale horizontal routing model to be coupled to land surface parameterization schemes." *Tellus* 48A:708–721.

Lundquist, J. D., and D. R. Cayan. 2007. "Surface temperature patterns in complex terrain: Daily variations and long-term change in the central Sierra Nevada, California." *Journal of Geophysical Research* 112: D11124, doi:10.1029 / 2006JD007561.

Lundquist, J. D., D. R. Cayan, and M. D. Dettinger. 2003. Meteorology and hydrology in Yosemite National Park: A sensor network application, in F. Zhao and L. Guibas (eds.), *Information Processing in Sensor Networks.* Springer-Verlag. 518–528.

Lundquist, J. D., D. R. Cayan, and M. D. Dettinger. 2004. "Spring onset in the Sierra Nevada—When is snowmelt independent of elevation?" *J. Hydrometeorology* 5:325–340.

Marks, D., J. Kimball, D. Tingey, and T. Link. 1998. "The sensitivity of snowmelt processes to climate conditions and forest cover during rain-on-snow—A case study of the 1996 Pacific Northwest flood." *Hydrological Processes* 12:1569–1587.

Maurer, E. P. and H. G. Hidalgo. 2008. "Utility of daily vs. monthly large-scale climate data: An intercomparison of two statistical downscaling methods." *Hydrol. Earth Syst. Sci.* 12:551–563.

Mazurkiewicz, A. B., D. G. Callery, and J. J. McDonnell 2008. Assessing the controls of the snow energy balance and water available for runoff in a rain-on-snow environment. Submitted to *Journal of Hydrology*. 55 p.

McCabe, G. J., M. P. Clark, and L. E. Hay. 2007. "Rain-on-snow events in the western United States." *Bulletin of the American Meteorological Society* 88:319–328, DOI:10.1175/BAMS-88-3-319.

Mo K. C., M. Chelliah, M. L. Carrera, R. W. Higgins, and W. Ebisuzaki. 2005. "Atmospheric Moisture Transport over the United States and Mexico as evaluated in the NCEP Regional Reanalysis." *Journal of Hydrometeorology* 6:710–728.

Mount, J., and R. Twiss. 2005. Subsidence, sea level rise, and seismicity in the Sacramento-San Joaquin Delta. San Francisco Estuary and Watershed Science 3, http://repositories.cdlib.org/jmie/sfews/vol3/iss1/art5.

Neiman, P. J., F. M. Ralph, A.B. White, D. A. Kingsmill, and P. O. G. Persson. 2002. "The statistical relationship between upslope flow and rainfall in California's coastal mountains: Observations during CALJET." *Mon. Wea. Rev. 130*:1468–1492.

Neiman, P. J., F. M. Ralph, G. A. Wick, J. D. Lundquist, and M. D. Dettinger. 2008a. "Meteorological characteristics and overland precipitation impacts of atmospheric rivers affecting the West Coast of North America based on eight years of SSM/I satellite observations." *J. Hydrometeorology* 9:22–47, doi:10.1175/2007JHM855.1.

Neiman, P. J., F. M. Ralph, G. A. Wick, Y. H. Kuo, T. K. Wee, Z. Ma, G. H. Taylor, and M. D. Dettinger. 2008b. "Diagnosis of an intense atmospheric river impacting the Pacific Northwest—Storm summary and offshore vertical structure observed with COSMIC satellite retrievals." *Monthly Weather Review* 136:4398-4420, doi:10.1175/2008MWR2550.1.

Neiman, P. J., A. B. White, F. M. Ralph, D. J. Gottas, and S. I. Gutman. In press. "A water vapor flux tool for precipitation forecasting." *Proceedings of Institution of Civil Engineers, Water Management Journal* (Special Issue on Weather Radar for Water Management). 16 p.

Nijssen, B., D. P. Lettenmaier, X. Liang, S. W. Wetzel, and E. F. Wood. 1997. "Streamflow simulation for continental-scale river basins." *Water Resour. Res.* 33(4): 711–724.

Nijssen, B., G. M. O'Donnell, D. P. Lettenmaier, D. Lohmann, and E. F. Wood. 2001. "Predicting the discharge of global rivers." *J. Clim.* 14:3307–3323.

Pandey, G. R., D. R. Cayan, and K. P. Georgakakos. 1999. "Precipitation structure in the Sierra Nevada of California during winter." *Journal of Geophysical Research* 104:12019–12030.

Rahmsdorff, S. 2007. "A semi-empirical approach to projecting future sea level rise." *Science* 368–370, doi:10.1126/science.1135456.

Ralph, F. M., P. J. Neiman, and G. A. Wick. 2004. "Satellite and CALJET aircraft observations of atmospheric rivers over the eastern North-Pacific Ocean during the winter of 1997/98." *Mon. Wea. Rev.* 132:1721–1745.

Ralph, F. M., P. J. Neiman, and R. Rotunno. 2005. "Dropsonde observations in low-level jets over the Northeastern Pacific Ocean from CALJET-1998 and PACJET-2001: Mean vertical-profile and atmospheric-river characteristics." *Mon. Wea. Rev.* 133:889–910.

Ralph, F. M., P. J. Neiman, G. Wick, S. Gutman, M. Dettinger, D. Cayan, and A. B. White. 2006. "Flooding on California's Russian River—Role of atmospheric rivers." *Geophysical Research Letters* 33(L13801), 5 p, doi:10.1029/2006GL026689.

Rogers, R. R., and M. K. Yau. 1989. *A short course in cloud physics*, 3rd ed. New York: Pergamon Press, 293 p.

Roos, M. 2006. "Flood management practice in northern California." *Irrigation and Drainage* 55:S93–S99.

Tarboton, D. G., and C. H. Luce. 1996. *Utah Energy Balance Snow Accumulation and Melt Model (UEB).* Computer Model Technical Description and Users Guide. 63 p.

Trenberth, K. E. 1999. "Conceptual framework for changes of extremes of the hydrological cycle with climate change." *Climatic Change* 42:327–339.

Weaver, R. L. 1962. *Meteorology of hydrologically critical storms in California*. Hydrometeorological Report No. 37. Washington, D.C.: U.S. Department of Commerce.

Wondzell, S. M., and S. G. King. 2003. Postfire erosional processes in the Pacific Northwest and Rocky Mountain regions. *Forest Ecology and Management* 178:75–87.

Wood, E. F., D. Lettenmaier, X. Liang, B. Nijssen, and S. W. Wetzela. 1997. "Hydrological modeling of continental-scale basins." *Annual Review of Earth and Planetary Sciences* 25:279–300. doi:10.1146/annurev.earth.25.1.279.

Wood, A. W., L. R. Leung, V. Sridhar, D. P. Lettenmaier. 2004. "Hydrologic Implications of Dynamical and Statistical Approaches to Downscaling Climate Model Outputs." *Climatic Change* 62:189–216.

Zhu, Y., and R. E. Newell. 1998. "A proposed algorithm for moisture fluxes from atmospheric rivers." *Mon. Wea. Rev.* 126:725–735.

8.0 Glossary

AR	Atmospheric Rivers
BDWM	Bay-Delta Watershed Model
CA	constructed analogues
cm	centimeter
cfs	cubic feet per second
CNRM	Centre National de Recherches Météorologiques
DJF	December, January, February
DWR	California Department of Water Resources
GCM	General Circulation Model
GFDL	Geophysical Fluid Dynamics Laboratory
GMT	Greenwich Mean Time
IPCC	Intergovernmental Panel for Climate Change
IWV	integrated water vapor
kg/m/s	kilograms per meter per second
km	kilometer
m	meter
MAM	March, April, May
mb	millibar
MJJ	May, June, July
mm	millimeter
m^3/s	cubic meters per second
NCAR	National Center for Atmospheric Research
NCEP	National Centers for Environmental Prediction
NOAA	National Oceanic and Atmospheric Administration
NSN	northern Sierra Nevada
PCM	Parallel Climate Model
SSM/I	Special Sensor Microwave/Imager
SSN	southern Sierra Nevada

USGS	United States Geological Survey
VIC	Variable Infiltration Capacity